TÉCNICO LISBOA

Hydrogen aircraft conceptual design and life cycle assessment

David Bernardo Da Silva Bico Pinto

Thesis to obtain the Master of Science Degree in

Aerospace Engineering

Supervisors: Prof. Frederico José Prata Rente Reis Afonso
Prof. Inês Esteves Ribeiro

Examination Committee

Chairperson: Prof. Paulo Jorge Coelho Ramalho Oliveira
Supervisor: Prof. Frederico José Prata Rente Reis Afonso
Member of the Committee: Prof. Ana Filipa da Silva Ferreira

July 2022

Dedicated to my grandfather, Dionisio, for all the love and for always believing in me.

Declaration

I declare that this document is an original work of my own authorship and that it fulfills all the requirements of the Code of Conduct and Good Practices of the Universidade de Lisboa.

Acknowledgments

First and foremost, I would like to express my deepest gratitude to my supervisors, Professor Frederico Afonso and Professor Inês Ribeiro for all the support and understanding that they provided and showed during the development of this dissertation.

I would also like to express my gratitude to all the Professors and colleagues that made this journey at Instituto Superior Técnico an unparalleled experience that shaped my life and myself.

Last but not least, I cannot find the words to express my gratitude towards my family and girlfriend, Ana, for all the emotional support and love that made this achievement possible.

Resumo

O setor da aviação é atualmente responsável por aproximadamente 2,4% das emissões antrópicas de CO_2 para a atmosfera. Tais emissões são inerentes à combustão de combustíveis à base de hidrocarbonetos (atualmente utilizados pela indústria aeronáutica). Como contramedida, nos Acordos de Paris, definiu-se enquanto meta a redução do aquecimento global para 1,5 graus Celsius comparativamente aos níveis pré-industriais.

O hidrogénio apresenta-se como uma forte alternativa aos combustíveis tradicionais, pois a sua combustão produz como produtos exclusivamente vapores de água e óxidos de nitrogénio (reduzindo até 90% as emissões de óxidos de nitrogénio quando comparado com combustíveis tradicionais).

A fim de quantificar os impactos ambientais desta transição e avaliar as modificações que uma aeronave propulsionada a hidrogénio sofreria, é realizado um projeto conceptual de uma aeronave propulsionada a hidrogénio e, seguidamente, realiza-se uma avaliação do ciclo de vida da produção de ambos os combustíveis mencionados. Uma avaliação económica dos diferentes combustíveis foi também realizada.

Relativamente à configuração da aeronave propulsionada a hidrogénio concluiu-se que esta aeronave teria um peso máximo à descolagem 3,37% inferior à aeronave de referência (Boeing 737-800) no entanto, de forma a acomodar os tanques criogénicos, o comprimento total da aeronave seria 22,56% superior à aeronave de referência.

Do ponto de vista ambiental é possível concluir que a implementação de hidrogénio enquanto combustível alternativo para a aviação levaria a uma diminuição das emissões de gases nocivos para a atmosfera. Particularizando para a utilização de hidrogénio verde, seria possível reduzir as emissões de CO_2-eq até 90,9% comparativamente aos combustíveis tradicionais.

Palavras-chave: Projeto conceptual de uma aeronave, Ciclo de vida, Tanques criogénicos, Hidrogénio.

Abstract

The aviation sector is currently responsible for approximately 2.4% of anthropogenic emissions of CO_2 into the atmosphere. Such emissions are inherent to the combustion of hydrocarbon-based fuels used in aviation. As a countermeasure, at the Paris Agreement, the reduction of global warming to 1.5 degrees Celsius compared to pre-industrial levels was set as a target.

Hydrogen presents itself as a strong alternative to traditional fuels, since it's combustion produces exclusively water vapors and nitrogen oxides as products (reducing up to 90% the emissions of nitrogen oxides when compared to traditional fuels).

In order to quantify the environmental impacts of this transition and assess the modifications that a hydrogen-powered aircraft would undergo, a conceptual design of a hydrogen-powered aircraft is realized and, posteriorly, a life cycle assessment of the production of both fuels is performed. An economic assessment of both fuels was also carried out.

Regarding the configuration of the hydrogen-powered aircraft, it was concluded that this aircraft would have a maximum take-off weight 3.37% lower than the reference aircraft (Boeing 737-800) however, in order to accommodate the cryogenic tanks, the total length of the aircraft would be 22.56% higher than the reference aircraft.

From an environmental point of view, it is possible to conclude that the implementation of hydrogen as an alternative aviation fuel would lead to a decrease in the emissions of harmful gases into the atmosphere. Particularly for the use of green hydrogen, it would be possible to reduce CO_2-eq emissions up to 90.9% compared to traditional fuels.

Keywords: Conceptual aircraft design, Hydrogen, Life cycle assessment, Cryogenic tanks.

Contents

List of Tables

List of Figures

Nomenclature

Greek symbols

ϵ	Emittance.
γ	Ratio of specific heats.
μ	Dynamic viscosity.
ν	Flight speed.
ϕ	Energy derivative.
ρ	Density.
σ	Allowable stress.

Roman symbols

c_p	Specific heat at constant pressure.
$\dot{m}$	Mass flow rate.
P	Power.
p	Pressure.
T	Temperature.
D	Drag.
d	Diameter.
e	Weld efficiency.
H	Enthalpy.
h	Heat coefficient.
K	Thermal conductivity.
L	Lift.
l	Length.

Nu Nusselt number.

Pr Prandtl number.

r Radius.

Ra Rayleigh number.

S Surface area of the tank.

u Internal energy.

V Volume.

W Mass.

y Fill level of the tank.

Subscripts

$LH_2{}'A/C - empty - notanks$ Empty Liquid hydrogen fuelled aircraft excluding cryogenic tanks.

$LH_2{}'A/C - empty$ Empty Liquid hydrogen fuelled aircraft.

$LH_2{}'A/C$ Liquid hydrogen fuelled aircraft.

∞ Free-stream condition.

Al Aluminium.

des Tank design/venting pressure.

g Gaseous physical state.

in Entrance of the control volume (tank or turbine for instance).

ins Insulation.

int Interior of the tank.

l Liquid physical state.

out Exit of the control volume (tank or turbine for instance).

$Ref'A/C - empty$ Empty Reference aircraft.

$Ref'A/C$ Reference aircraft.

s Cylindrical shaped part of the tank.

t Tank.

TO Take-off.

w Tank wall.

Glossary

APU - Auxiliary Power Unit

ASME - American Society of Mechanical Engineers

ATAG - Air Transport Action Group

ATLRS - Aircraft Top Level Requirements

CCS - Carbon Capture and Storage

CH_4 - Methane

CO - Carbon Monoxide

CO_2 - Carbon Dioxide

CORSIA - Carbon Offsetting and Reduction Scheme for International Aviation

CSD - Compression Storage and Dispensing

ESFC - Energy Specific Fuel Consumption

FCU - Fuel Control Unit

FEM - Finite Element Method

GH_2 - Gaseous Hydrogen

GHG - Greenhouse Gasses

GWP - Global Warming Potencial

H_2 - Hydrogen

H_2O - Water

HFCU - Hydrogen Fuel Control Unit

IATA - International Air Transport Association

IPCC - Intergovernmental Panel on Climate Change

LCA - Life Cycle Assessment

LCH_4 - Liquid Methane

LDI - Lean Direct Injection

LH_2 - Liquid Hydrogen

MIT - Massachusetts Institute of Technology

MLI - Multi Layer Insulation

MTOW - Maximum Take-Off Weight

N_2 - Nitrogen

NIST - National Institute of Standards and Technology

NGV - Nozzle Guide Vanes

NO - Nitric Oxide

NO_x - Nitrogen Oxides

O_2 - Oxygen

O&M - Operations and Maintenance

PV - Photo Voltaic

PEM - Polymer Electrolyte Membrane

R&D - Research and Development

SFC - Specific Fuel Consumption

SFO - San Francisco International Airport

SO_x - Sulfur Oxides

SMR - Steam Methane Reforming

TET - Turbine Entry Temperature

UHC - Unburned Hydrocarbons

Chapter 1

Introduction

1.1 Motivation

The global aviation sector is currently responsible for approximately 2.4% of anthropogenic carbon dioxide (CO_2) emissions to the atmosphere [1]. Moreover, according to the Air Transport Action Group (ATAG), 80% of all aviation sector emissions have their origin in flights of over 1 500 miles (medium to long haul flights). Regarding solely the transport paradigm, the aviation sector represents a significant 12% of CO_2 emissions to the atmosphere in this sector [2].

Khandelwal et al. states that the aviation industry is projected to be the fastest growing industry for the next decades [3], and according to Lee et al., despite the COVID-19 pandemic impact on aviation, aviation traffic is likely to recover to the projections earlier to the pandemic [1] (figure 1.1 presents a projection of the GDP growth for this industry). As such, this growing industry and it's inherent emissions are in direct conflict with the global descarbonization goals [4].

The sum of CO_2 and non-CO_2 emissions cause a warming of the Earth's surface. The most significant contributor to anthropogenic climate change is the increasing concentration of CO_2, which is considered the prime cause for the global warming in recent years [4]. In order to encourage a reduction in emissions, the International Air Transport Association (IATA) has set the goal to reduce global aviation sector emissions by an amount of 50% until the year of 2050, comparing with emission levels of 2005 [5]. Also, at The Paris Agreement, a goal was set to reduce global warming to 1.5 degree Celsius comparing to pre-industrial levels, which would bring several environmental and human health benefits [6].

The burning of hydrocarbons releases several pollutants to the atmosphere, such as carbon monoxide (CO), CO_2, nitrogen oxides (NO_x), soot, unburned hydrocarbons (UHC) and sulfur oxides (SO_x) [7]. The previous species of pollutants must be reduced in order to achieve the targets mentioned above. Hydrogen fuel can prove a suitable alternative fuel since it is free of carbon and other impurities [3]. Hydrogen is also the most abundant element on the universe, unlike fossil fuels, which are debated to be exhausted sometime during this century [3]. Furthermore, hydrogen combustion produces only water vapor (H_2O) and NO_x [7].

Bearing in mind that the increase of CO_2 is the main contributor to climate change in recent years,

and also, that hydrogen fuel combustion has no CO_2 emissions, it's position as an alternative fuel to kerosene fuel strengthens.

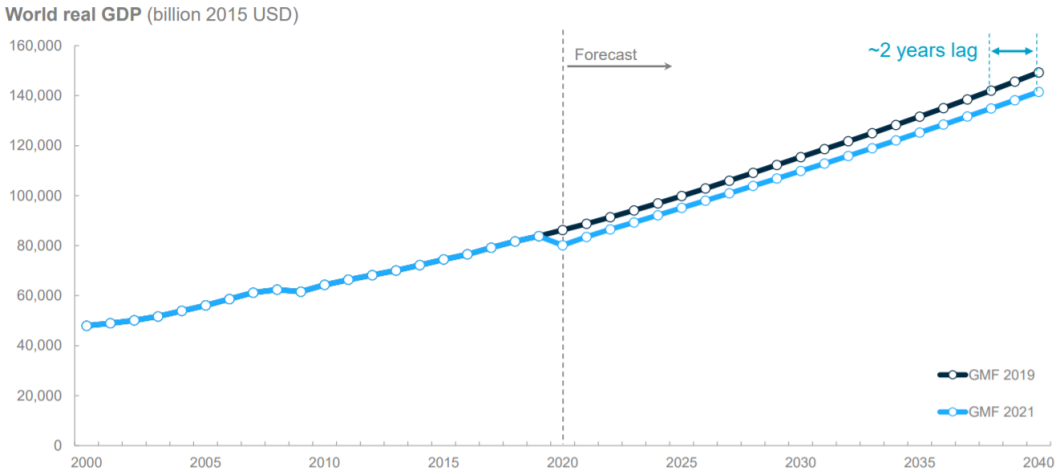

Figure 1.1: Forecast 2021 - 2040 for aviation sector GDP growth [8]

1.2 Objectives

This thesis sets itself the objective of sizing a conceptual liquid hydrogen fuelled aircraft (LH_2 aircraft) in order to infer whether or not the implementation of liquid hydrogen as an aviation fuel would prove environmentally superior to traditional aircraft in terms of environmental impacts.

In order to assess the environmental impacts of implementing a liquid hydrogen fuelled aircraft a life cycle assessment is to be performed for different hydrogen production methods and also for kerosene fuel.

Finally, an economic assessment is to be performed in order to assess the economic competitiveness of hydrogen versus kerosene fuel.

1.3 Thesis Outline

In order to address the objectives set for this thesis, the following structure has been adopted:

Chapter 1 - Introduction:

This chapter provides the reader with the motivation behind this research theme and sets the main objectives.

Chapter 2 - Implications and design changes due to liquid hydrogen transition:

This chapter contains the background related to the history of hydrogen usage in the aviation sector, impacts of pollutants on the environment and the inherent aircraft, airport and systems modification that stem from the transition of conventional aircraft to LH_2 fuelled aircraft.

Chapter 3 - Design requirements:

This chapter provides a brief introduction to the fundamentals of conceptual aircraft design.

Chapter 4 - Implementation:

This chapter details the theoretical design of the cryogenic LH_2 tanks, the sizing of the conceptual LH_2 aircraft and also, it sets the basis for the LCA.

Chapter 5 - Results & discussion:

This chapter presents and discusses the results obtained for the conceptual LH_2 fuelled aircraft and the LCA. It also assesses the economic competitiveness of LH_2 in comparison with kerosene fuel.

Chapter 6 - Conclusions:

This chapter summarizes all the conclusions derived from this study and entails future work.

Chapter 2

Implications and design changes due to liquid hydrogen transition

2.1 Liquid hydrogen vs kerosene fuel properties

According to the table below, LH_2 fuel has a specific energy about 2.8 times higher when compared to the currently utilized jet A (kerosene) fuel. However, kerosene fuel is the fuel which displays the highest energy density, in other words, for the same energy content, LH_2 fuel requires four times more volume than kerosene fuel.

Table 2.1: Physical properties of liquid hydrogen at boiling point and kerosene, values gathered from [9] and [10].

Property	Unit	LH_2	Kerosene
Molecular weight	Kg/mol	$2.016 \cdot 10^3$	$168 \cdot 10^3$
Temperature	K	20.369	439.817
Heat of combustion	J/Kg	$120 \cdot 10^6$	$42.798 \cdot 10^6$
Density	Kg/m^3	70.9	810.53
Specific heat capacity	J/KgK	$9.747 \cdot 10^3$	$1.968 \cdot 10^3$
Specific energy	MJ/Kg	122.8	42.8
Energy density	$MJ \cdot Kg/m^3$	8706.52	34690.68

Comparatively to it's competitor, LH_2 has several advantages. It can be produced at a given rate because its primary source is water (water is a renewable resource), and as a result of combustion it only releases H_2O and small quantities of NO_x (please visualize figure 2.1 to apprehend the total array of chemical species emitted from the combustion of both fuels) [11]. In fact, the combustion of LH_2 fuel can produce up to 90% less NO_x emissions [12].

Another useful property that hydrogen has compared to hydrocarbon fuels is it's flammability range, which allows it to be used in a wide range of margins, thus promoting the previously mentioned lower emissions of NO_x. It also promotes the use of smaller engines, thus enabling engines to be quieter [11].

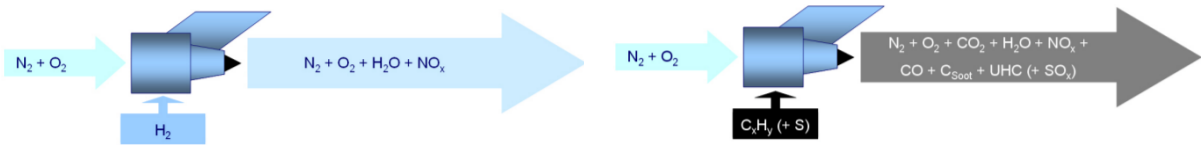

(a) LH_2 fuel combustion emissions (b) kerosene fuel combustion

Figure 2.1: Species emitted by the combustion of LH_2 and kerosene fuel upon aircraft operation [13].

2.2 Historical overview

Hydrogen (H_2) was first used in aeronautics as a substitute for hot air in balloons. The first hydrogen-lifted balloon was constructed in France by the Roberts brothers under the supervision of the physicist Jacques Charles. It made its maiden flight in Paris in August 1783 at an altitude of 900 m and traveled a distance of 24 km for about 45 min [14].

In the 19th century, count Ferdinand Von Zeppelin made use of hydrogen in order to create enough buoyancy for his rigid frame airship (figure 2.2), which was named after himself. The first flight of the Zeppelin took place on the 2nd of July 1900 over Lake Constance. Damaged during landing, it was repaired and modified and proved its potential in two subsequent flights made on the 17th and the 24th of October 1900 [19], bettering the 6 m/s (21.6 km/h) velocity attained by the French airship La France [15].

In 1937, Hans Von Ohain developed the Hes 1 engine which was powered by hydrogen consisting in a back to back radial compressor and a radial inflow turbine [16].

After the flights of the zeppelin rigid frame airships, in 1956, the American bomber B-57 used in one of its dual engines a combination of hydrogen and helium, where the latter was used to pressurize the hydrogen. The engine used for this test was a modified J-65 engine to accommodate the injection of hydrogen [17]. Later, in 1988, Soviet scientists led experiments on a modified TU-154 (afterwards renamed as TU- 155) where one of it's two engines operated using hydrogen as fuel. Important experimental results were provided by this experiment regarding aircraft operation and safety that helped bringing the usage of hydrogen as fuel closer to traditional aviation standards [11].

Soviets and Germans united in 1991, setting themselves the goal of designing a commercial aircraft fuelled by liquid hydrogen. This aircraft was similar to the Airbus A310 and the TU-204, featuring 200 passengers, dual engines and an estimated range of 500 miles. As a result of this study, the liquid hydrogen tanks were placed on top of the fuselage and a small portion was also placed on the wings. Meanwhile, NASA was also developing it's own prototype of a LH_2 fuelled aircraft but in this case, the LH_2 tanks were spherical and placed within the fuselage of the aircraft [11].

The CRYOPLANE project was launched in the year of 2000 and consisted in a consortium of 35 entities of relevant areas from 11 different European countries led by Airbus Deutschland. This "system analysis" was scheduled to last for 2 years and it's main purpose was to set the basis for future investigation regarding the topic of liquid hydrogen fuelled aircraft. In order to achieve this, the research covered relevant technical and strategic aspects. Properties such as aircraft configurations for all commercial

ranges, propulsive cycles, airport infrastructure and environmental compatibility were studied [18].

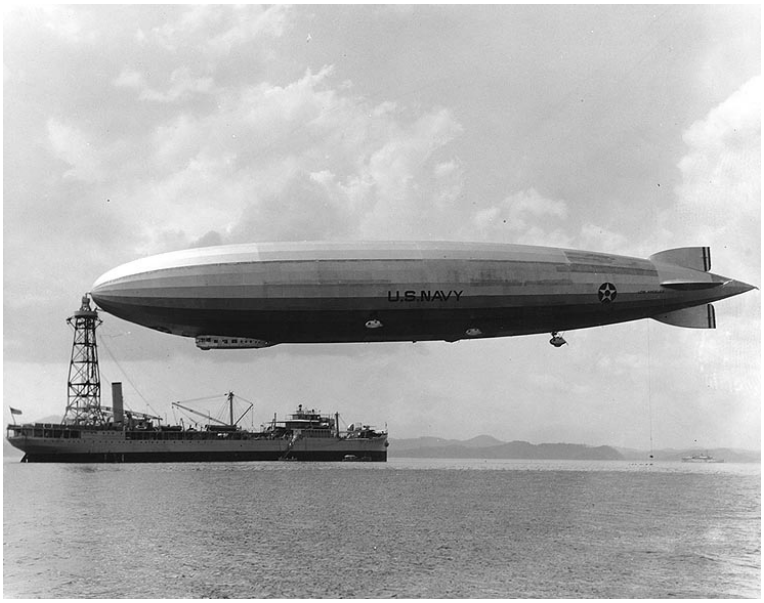

Figure 2.2: USS Los Angeles, an American airship built in Germany by the Luftschiffbau Zeppelin [19].

2.3 Environmental impact of pollutants

The bulk of aircraft emissions due to fuel combustion are CO_2 and H_2O, both of which are considered greenhouse gasses (GHG). Other significant gasses emitted to the atmosphere are nitric oxide (NO) along with nitrogen dioxide (NO_2), commonly referred together as NO_x. SO_x and soot are also emitted to the atmosphere [20].

Globally speaking, the presence of GHG such as CO_2, CH_4, NO_x and H_2O in the atmosphere have been increasing at an unseen rate since the industrial revolution due to both economic and population growth factors (please visualize figure 2.3). At the current date these GHG have reached unprecedented atmospheric concentration levels and are linked to the observed warming of the planet's surface since the 1950's [21].

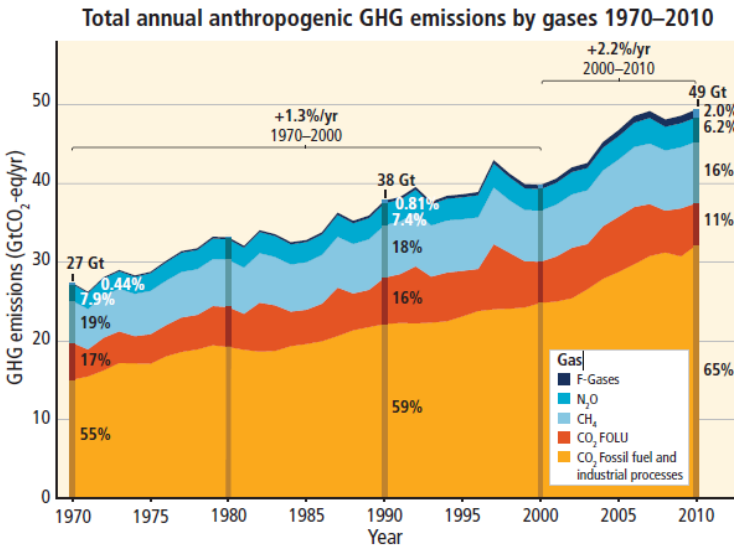

Figure 2.3: Concentration of GHG in the Earth's atmosphere, adapted from [21].

The impacts of the climatic changes derived from the elevated concentration levels of GHG in the atmosphere are felt the strongest in natural systems. For instance, the change in precipitation in some regions as well as the melting of ice provoke alterations in hydrological systems translating into fluctuations of quality and quantity of the water available. Also according to the 2014 IPCC technical report [21], many terrestrial, fresh water and marine species have changed their behaviour due to the climatic changes. Ocean acidification and warming as a result of direct human activity has also been proven.

As a result of global warming it is expected an increase in the frequency displayed by extreme events, also, extreme events related with high temperature will be more and more frequent than extreme events related to low temperatures [21].

Moreover, if the emissions of GHG to the atmosphere remain unchecked, further warming is to be expected, which in turn can cause irreversible damage for people and ecosystems [21]. Figure 2.4 illustrates a prediction of the average surface temperature in a few decades.

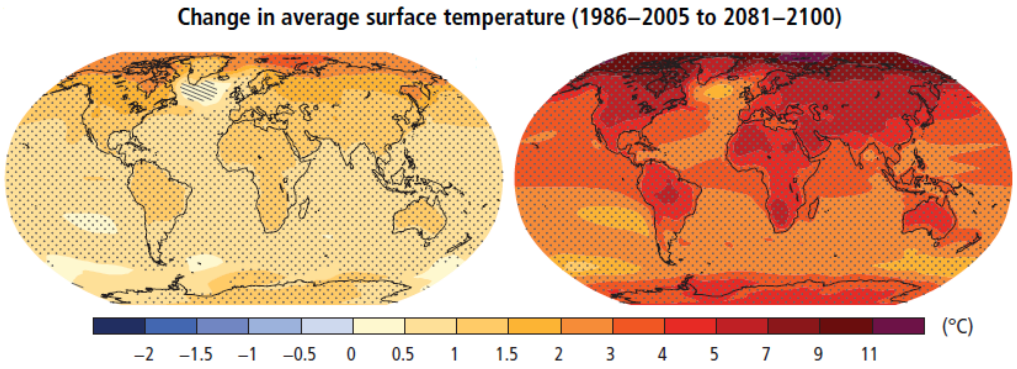

Figure 2.4: Evolution of the average temperature of Earth's surface prediction, adapted from [21].

2.4 Hydrogen production

Hydrogen is indeed, as stated before, a very promising alternative fuel in order to reduce the emissions of GHG and other nocive gasses to the environment. As such, in order to attain the full picture of what would mean to transit from fossil fuels to hydrogen fuel, the sights must also be set to the inevitable impacts of hydrogen production.

Hydrogen production processes may in fact be damaging to the environment if the primary energy source is a fossil fuel. However the definition is more complex than this, according to Minli Yu et al. [22], there are four classifications regarding hydrogen as a final product given it's production path, which are green hydrogen, aqua hydrogen, blue hydrogen (all of these are low carbon) and grey hydrogen. Green hydrogen is a hydrogen final product where it's primary energy source is renewable. Blue hydrogen, contrary to green hydrogen, is a classification given to hydrogen produced with a fossil fuel as a primary energy source, however, there must be CO_2 capturing technologies in place. Aqua hydrogen uses fossil fuels as a primary energy source, however, the technologies involved in it's production produce no CO_2 emissions. Lastly, grey hydrogen is produced using fossil fuels as a primary energy source, however there are no CO_2 retention or no zero CO_2 emission technologies in it's processes, as such, this pathway could potentially be more impactful to the environment. This master thesis will be focusing in grey, blue and green hydrogen production pathways.

Although it is much more desirable to obtain hydrogen from low carbon renewable resources since there is very little impact on the environment [23], these "greener" sources of hydrogen production lose some of their attractiveness due to high cost and low efficiencies [24].

In the present day 48% of all hydrogen is produced by steam methane reforming (SMR), the second and third most significant hydrogen production methods are oil reforming and coal gasification with a share of 30% and 18% respectively. Given the previous statement one can infer that about 96% of all available hydrogen is produced with fossil fuels as it's primary energy source [24].

According to the United States of America Department of Energy [25] the processes used to produce hydrogen can be divided into thermochemical processes, biological processes, electrolytic processes and direct solar water splitting processes. Thermochemical processes are characterized by combining heat and chemical reactions to retrieve hydrogen from organic materials and water. Biological processes are characterized by the production of hydrogen due to bacteriological and microalgae activity under direct sunlight or fed by organic matter. Electrolysis consists in the splitting of water into hydrogen and oxygen. This feat can be achieved by the use of electrolyzers, which require electricity to perform the split. Direct solar water splitting process, also called photolytic process, uses direct exposure to sunlight energy to split water into hydrogen and oxygen, this technology however is still at the research level.

Some examples of the processes previously mentioned are illustrated in the table 2.2:

Table 2.2: Hydrogen production methods.

Process mechanism	Processes
Thermochemical	Steam gas reforming (SMR) Coal gasification Biomass gasification Biomass-derived liquid reforming Solar thermochemical hydrogen
Biological	Microbial biomass conversion Photobiological
Electrolytic	Electrolysis
Direct Solar Water Splitting	Photoelectrochemical Photobiological

It is also important to note that one specific process can be fed by different kinds of feedstock, for instance, for the specific case of hydrogen production by water electrolysis, the electricity needed for the electrolytic process can be originated from a renewable energy source, such as wind or solar energy, or it can have it's origin in fossil fuel or even nuclear power. The different pathways for hydrogen production can have differing environmental impacts as it will be explained on the next chapters of this thesis.

The previously explained phenomena can be further analyzed on the schematic below (figure 2.5) retrieved from Khandelwal et al [3].

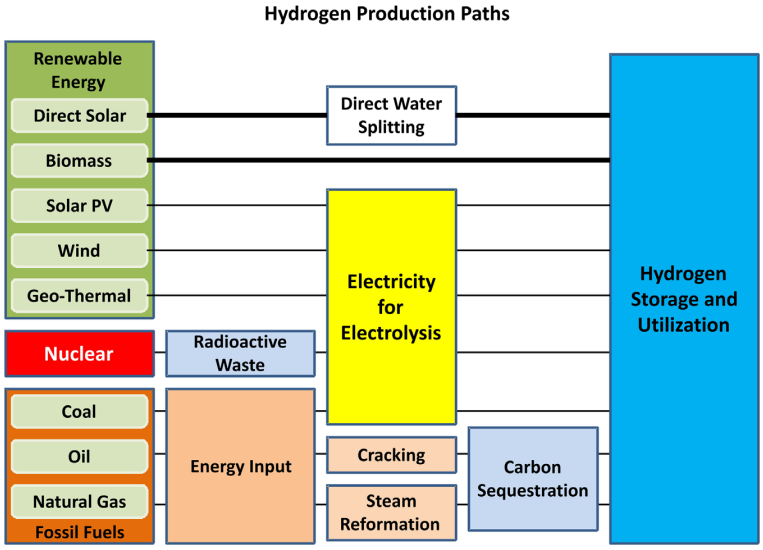

Figure 2.5: Map of production pathways for hydrogen [3].

2.5 Aircraft design

According to Cryoplane's project final report [26], the main driver for a LH_2 aircraft's design is in fact the layout of the cryogenic tanks since LH_2 requires four times more storage volume capacity than a traditional kerosene aircraft for the same energy content, moreover, the pressurization of LH_2 leads to heavier tanks than those used to storage kerosene fuel. The possibility of installing the cryogenic tanks

on the wings was also explored on this report, however calculations showed that this solution would result in a quite heavy structure and thus it was considered unfeasible.

Three main cryogenic tank layouts were devised, mainly constricted by the need to maintain the aircraft's balance around it's center of gravity [26]:

- For smaller aircraft, it is feasible and ideal to place the cryogenic tank located behind the aft pressure bulkhead, as it is illustrated in figure 2.6 a).
- Medium range aircraft, due to increased fuel fraction, require the placement of a cryogenic tank at the top of the fuselage in order to balance the cryogenic tank located behind the aft pressure bulkhead. Otherwise there would have to be an increase in the area of the horizontal tail. The detailed schematic for this configuration can be visualized in figure 2.6 b).
- The last cryogenic tank layout is devised to address long range aircraft. As it can be seen in the cross sectional view of the cabin of figure 2.6 c), two tanks can be placed within the fuselage, one tank behind the aft pressure bulkhead and another tank between the cockpit and the cabin. The forward cryogenic tank will be crossed by a catwalk in such a way that it ensures a connection between the cockpit and the cabin.

Airbus project ZEROe (still in development) selected the configuration that features the placement of the cryogenic tank behind the aft pressure bulkhead for it's medium range conceptual aircraft [27]. This thesis will follow the same approach regarding the conceptual design of the LH_2 fuelled aircraft.

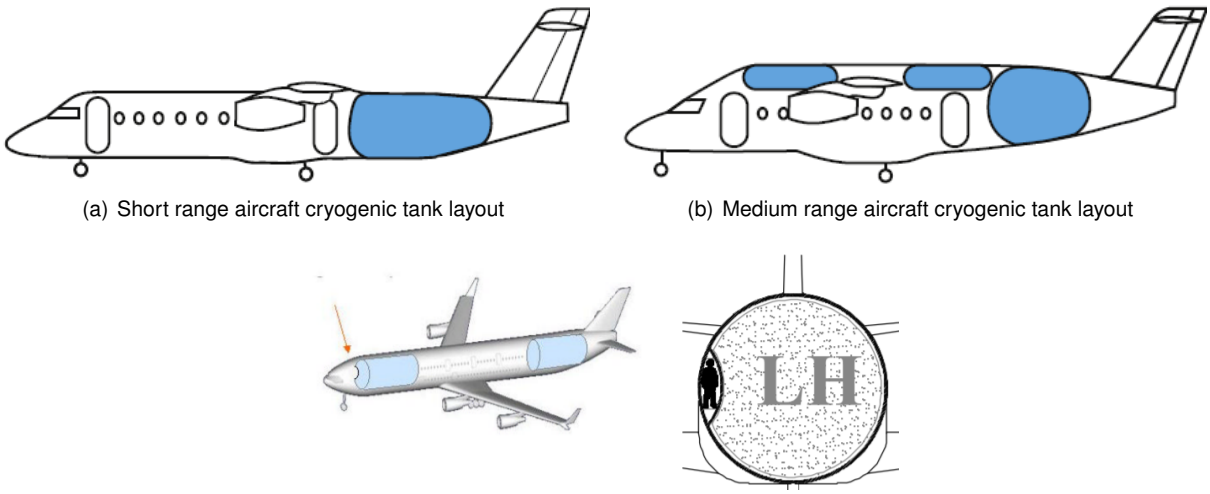

(a) Short range aircraft cryogenic tank layout

(b) Medium range aircraft cryogenic tank layout

(c) Long range aircraft cryogenic tank layout

Figure 2.6: Three main cryogenic tank layouts proposed in cryoplane's project final report, adapted from [26] and [28].

2.6 Airport design and operations

Between the dates of 1975 and 1976, interest started to arouse regarding what facilities should be present at airports in order to enable LH_2 fuelled commercial aircraft. To tackle this question, NASA

awarded parallel contracts to Lockheed Martin Corporation and Boeing. Each contract foresaw the study of the implementation of LH_2 fuel system in a major airport. Both studies had similar conclusions, as such, San Francisco's International Airport (SFO) conclusions will be highlighted here [29].

The study concluded that for a peak season in SFO, 731 tons of LH_2 per day would be needed. However, in order to account for the boil-off phenomena, this number rises to 836 tons of LH_2 per day. In other words, SFO airport would need to create the capacity to liquefy 836 ton of LH_2 per day, thus constraining the minimal liquefying facility capacity [29]. As a side note, given the growth of the aviation industry since 1976, this airport would need a higher liquefying capacity to cope with present day needs.

Regarding the location of the liquefaction plant, it is economically more beneficial to locate the liquefaction plant on the airport itself and feed the plant with GH_2 transported by pipelines from it's production origin. In case it is physically impossible to locate the liquefaction facility on the airport, the most economically competitive method is to transport the LH_2 via vacuum-jacketed pipelines up to 40 miles. For distances greater than 40 miles, the best method is to transport LH_2 by railroad tankcar [29].

As for the storage of LH_2, several tank designs were studied and it was concluded that the best option is to store the LH_2 in underground spherical tanks possessing a vacuum insulated double wall with perlite filling the evacuated annulus. This insulation system proved to be the best economic solution even accounting for boil-off losses of LH_2 during it's 30 year life span [29].

A loop circuit of continuously pumped LH_2 should be implemented around the airport in order to assure the availability of subcooled LH_2 at anytime and at any gate position (see figure 2.7). The continuous feed of LH_2 by pumps proved to be several times more effective than LH_2 feed by pressure in minimizing boil-off [29].

Aircraft should be refuelled by accessing the tail cone where it is possible to connect two ground-based hoses available at the gate. One ground-based hose is responsible for the supply of LH_2, the other hose captures the GH_2 that is present inside the aircraft's tank [29].

When an aircraft undergoes maintenance activities, the LH_2 should be removed from the tank, then GH_2 is expelled from the tank with nitrogen (N_2). After a slight warm up of the cryogenic tank, the N_2 is replaced with air. Regarding the refuelling of the aircraft, N_2 is used to purge the air and it's moisture from the tank, then the N_2 is replaced by GH_2 and subsequently, the tank is cooled, finally this tank is filled with LH_2 [29].

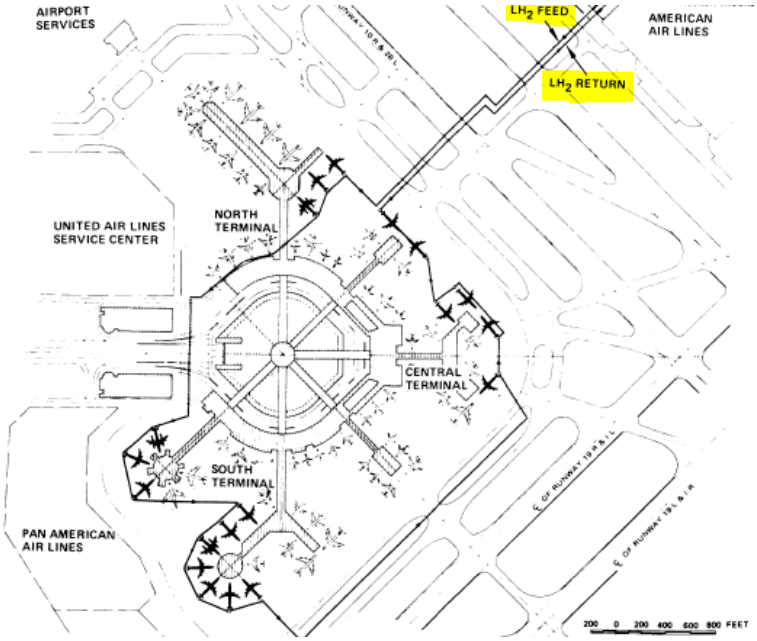

Figure 2.7: Airport continuous fuel loop for every gate [29]

2.7 Safety

According to Brewer [29], a crash test study was carried with an aircraft fuelled with four different fuels, LH_2, liquid methane (LCH_4), Jet A and JP-4. The purpose of this test was to assess the damage that would result for each of the previously mentioned fuels to the aircraft's passengers and surroundings. Three types of crashes were studied, two of them were considered survivable and one was not. The purpose of the unsurvivable crash was to assess the damage that the fuels would impose on it's surroundings. For each type of crash LH_2 fuelled aircraft was able to outperform all the other fuels tested [29].

The positive results obtained by the LH_2 aircraft can be explained in part by the lesser susceptibility that LH_2 tanks present to damage. This higher resistance to damage is a result of the structural protection that it possess, making a puncture less likely to occur. In case of a large spilling, LH_2, evaporates and dissipates into the atmosphere at a higher pace than the other fuels, thus leading to lesser damage to the passengers and it's surroundings. Another important argument is that in case of ignition, the fire will go extinct quite faster than other fuels, this will promote less damage to the fuselage since it will not be heated to the point of structural collapse [29].

2.8 Liquid Hydrogen tank theoretical design

With the use of hydrogen as a fuel at cryogenic temperatures, there is the inherent need for creating dedicated devices to storage this fuel. Hydrogen could be stored in its gaseous state, however this would render the cryogenic tanks heavier than those needed to store LH_2. Solid hydrogen would demand high quantities of energy to subcool the fuel and it would only lead to small gains in cryogenic tank weight

reduction. Hydrogen storage as supersaturated liquid would create higher pressure fluctuations inside the tank, thus leading to heavier tanks. As such, storage as saturated liquid is the optimal solution [28].

Tank shape

Spherical tanks have been in use for a few decades in space applications, since this particular shape requires less surface area for any given volume. The reduction in surface area diminishes the passive heat flux into the cryogenic tank, thus resulting into a smaller boil-off rate (vapours created due to heat input from the environment [30]). Cylindrical cryogenic tanks possess a higher surface area to volume ratio than spherical tanks, thus leading to a higher fuel loss due to boil-off. However, cylindrical tanks are easier to manufacture and can be better integrated in the aircraft's fuselage [3].

Tank configuration

There are two types of configurations in relation to the aircraft for hydrogen tanks, integral tanks and non-integral tanks.

Non-integral cryogenic tanks are typically mounted into a conventional fuselage or wings and as a result these tanks are only subjected to aerodynamic loads, fuel dynamic loads and thermal loads.

Integral tanks are in fact an integral part of the aircraft's air frame, and due to this fact, an integral tank is expected to endure axial, bending and shear stresses that are inherent to a fuselage [7]. The schematic below (figure 2.8) illustrates how the tank structure (or wall), insulation and outer fuselage come together in an integral tank configuration. This work will consider integral tanks as basis for it's calculations.

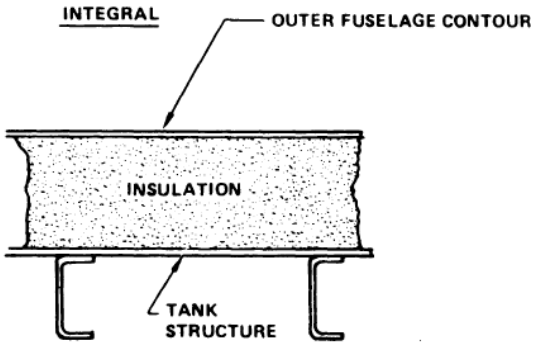

Figure 2.8: Integral tank schematic, adapted from Brewer [29]

Tank wall

The tank walls need to be comprised, ideally, by a material that possess characteristics such as high strength, high fracture toughness and high stiffness. This ideal material should also display low density and low permeation to LH_2 and GH_2 [31].

Fracture toughness is of particular importance since this material will be subjected to cryogenic temperatures, which renders many materials brittle. Aluminium alloys are a strong candidate due to low susceptibility to hydrogen embrittlement [28]. Composite materials are also a viable option given the fact that hydrogen permeability is no longer an issue with these materials and the usage of composites

would results in a weight saving of 25% for the tank wall [28].

Tank insulation

The tank insulation must be as lightweight and efficient as possible to properly store the LH_2 since an optimal insulation criteria results in minimal boil-off, which is of particular importance for longer duration applications such as commercial aviation [7]. Thus, the insulation material must display low thermal conductivity. It must also possess a low thermal diffusivity and low mass density [31]. Foams, aerogels and multilayer insulation systems (MLIs) all display the necessary characteristics before mentioned [31]. Vacuum insulation systems could also provide good insulation, however using such system would increase the tank weight, since the vacuum would have to be created between two tank walls, additionally, this type of insulation system has no resistance to radiation heat transfer [31]. According to Verstraete et al. [28] aerogels are fragile and brittle given their high porosity, as such, their use in a cryogenic tank application is not ideal.

MLI systems consist in several alternating layers of a low conductivity spacer and a foil with low emissivity. Also, to minimize heat conduction due to residual gasses, MLI must operate at high vacuum levels below 13 mPa [28].

The insulation material can either be placed on the exterior of the cryogenic tank or inside the tank, directly in contact with the LH_2 and GH_2. If the insulation is placed inside the tank, the efficiency of the insulation may be crippled due to increased heat conductivity caused by the diffusion created by the GH_2. Interior insulation also imposes the necessity of material impermeability to GH_2, thus, further constraining the insulation material selection task [3].

Figure 2.9 illustrates a cylindrical LH_2 tank with semi-spherical heads insulated by foam.

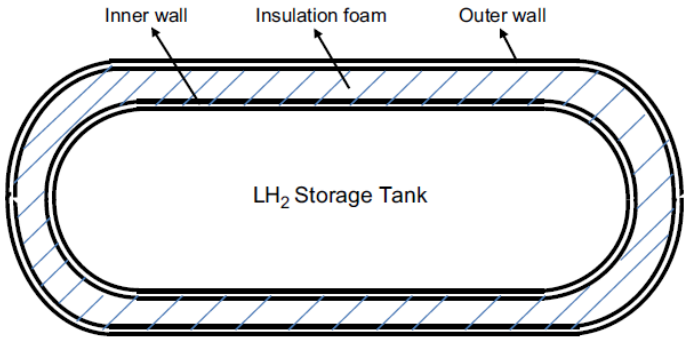

Figure 2.9: Foam insulated tank schematic, adapted from Khandelwal et al. [3]

2.9 Engine performance and design

As seen in previous sections, the combustion products of hydrogen are very different from those of hydrocarbon combustion. This difference is vital for the understanding of this section, and taking this into account, the chemical reactions of both the combustion of hydro-carbon and the combustion of hydrogen, respectively, are presented below:

$$C_{12}H_{23} + 17.75\,O_2 + 66.77\,N_2O_2 \longleftrightarrow 12\,CO_2 + 11.5\,H_2O + 66.77\,N_2 \tag{2.1}$$

$$2\,H_2 + O_2 \longleftrightarrow 2\,H_2O \tag{2.2}$$

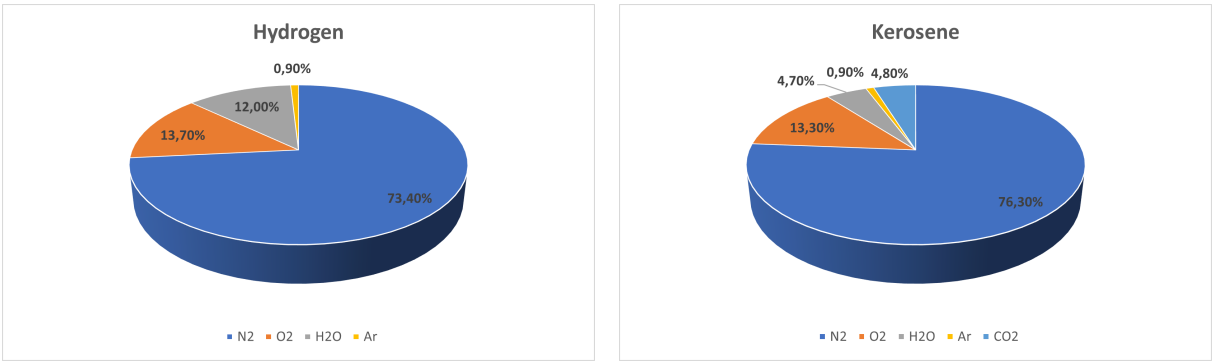

(a) Hydrogen combustion gases.

(b) Kerosene combustion gases.

Figure 2.10: Combustion products and respective ratios, adapted from [32].

The previous chemical reactions are presented in their stoichiometric form and do not include other chemical species that are usually present in very high temperatures reactions (as illustrated in figure 2.1), if the reader is compelled to further investigate these reactions in detail it is advised to read references [33] [34].

Observing equations (2.1) and (2.2) it is clearly visible that water vapor is a product of both chemical reactions, however, according to Verstraete [7] and Boggia [32] there is a higher percentage of H_2O present in the aftermath of the hydrogen combustion (figure 2.10).

Since there is more quantity of H_2O in the product gasses of a hydrogen combustion and adding to the fact that H_2O has a high specific heat, it can be stated that hydrogen combustion has a higher specific heat when compared to equivalent gasses from hydro-carbon combustion [7]. As a direct result from hydrogen's combustion having a higher specific heat, the turbine expansion in the reactor (engine) is modified, leading to a benefit of about 3% in energy specific fuel consumption (ESFC) when compared to hydrocarbon combustion, as Verstraete [7] also states.

Figure 2.11 further illustrates the significant difference between hydrogen fuel and, as a representative of hydro-carbon fuels, kerosene fuel. The higher specific heat of hydrogen combustion will induce some alterations to the power output of the turbine, however, the power output of the turbine will remain balanced as it will be demonstrated with the help of propulsion principles [35]:

$$\dot{m}_{turbine} = \dot{m}_{air} + \dot{m}_{fuel} \tag{2.3}$$

The previous equation represents the turbine mass flow rate, $\dot{m}_{turbine}$, where $\dot{m}_{air}$ stands for the mass flow rate of air and finally, $\dot{m}_{fuel}$ represents the mass flow rate of fuel. Using the turbine mass flow

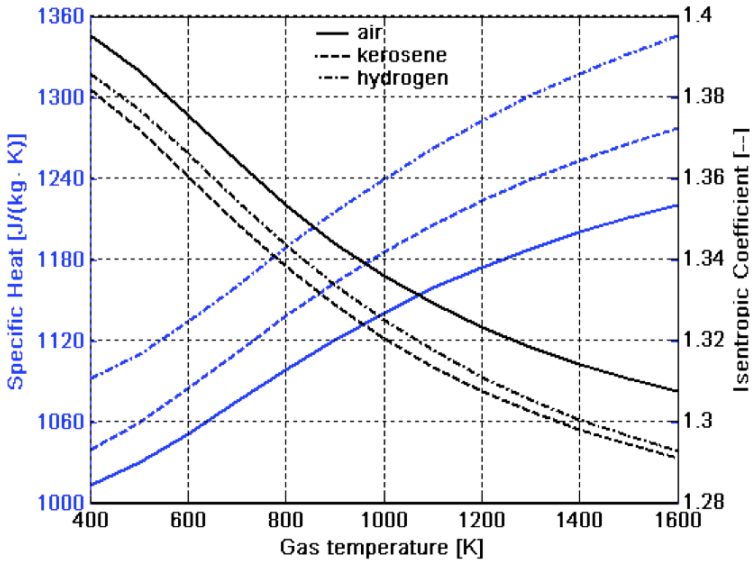

Figure 2.11: Specific heat for hydrogen and kerosene fuels [7]

rate it is now possible to calculate the turbine power using the following expression:

$$P_{turbine} = \dot{m}_{turbine} \times c_p \times (T_{in} - T_{out}) \tag{2.4}$$

In equation (2.4) c_p is the specific heat at constant pressure, T_{in} and T_{out} are the temperatures of the gas at the entrance of the turbine and at the exit of the turbine respectively.

According to propulsion fundamentals, the following relation can be made [35]:

$$c_p \times (T_{in} - T_{out}) = H_{in} - H_{out} \tag{2.5}$$

where H_{in} and H_{out} represent the enthalpy at the entrance and exit of the turbine, respectively. Substituting equation (2.5) in equation (2.4) the following equation is obtained:

$$P_{turbine} = \dot{m}_{turbine} \times (H_{in} - H_{out}) \tag{2.6}$$

Given that the hydrogen combustion gasses have higher specific heat than the gasses produced from the combustion of kerosene (as shown in figure 2.11) it implies that the temperature at the exit of the turbine, T_{out}, will be higher for the combustion of hydrogen and thus, the enthalpy at the exit of the turbine, H_{out}, will also be higher (meaning a smaller enthalpy drop than for kerosene combustion). Although, equation (2.6) will remain balanced due to lower mass flow rate of the turbine. This reduction of the mass flow rate of the turbine is a consequence of the reduced fuel flow of hydrogen fuel [7].

Verstraete [7] also states that the ratio of specific heats, γ, changes in the case of hydrogen combustion, becoming higher than the value for kerosene combustion. As consequence of a higher ratio of specific heats, the pressure drop along the turbine will also be smaller for hydrogen combustion, this result is supported by the equation below:

$$\frac{T_{out}}{T_{in}} = \left(\frac{p_{out}}{p_{in}}\right)^{\frac{\gamma-1}{\gamma}} \tag{2.7}$$

Since, according to equation (2.7) and attending to the knowledge that the γ is higher than for kerosene, the gasses resulting from the combustion of hydrogen will have more energy after the turbine, thus the thrust will also be higher than when using kerosene.

On the other hand, there is also a different approach. Instead of keeping the temperatures T_{in} and T_{out} equal for both the burning of hydrogen and kerosene, thus promoting a higher thrust (under the same conditions of temperatures at the turbine) for the hydrogen combustion, one can decrease the temperature at the entrance of the turbine, T_{in} (also know as TET) up to 50k [32]. The decreasing of TET, will promote a life expectancy increase for the engine, particularly for the turbine blades.

2.9.1 Potential improvements to engine thermodynamic cycle

According to Boggia [32], since there is LH_2 present in the aircraft, it can be used for more applications than only the burning of fuel. These possible changes are applied to the conventional thermodynamic cycle and as a result, it is obtained something called as an unconventional engine.

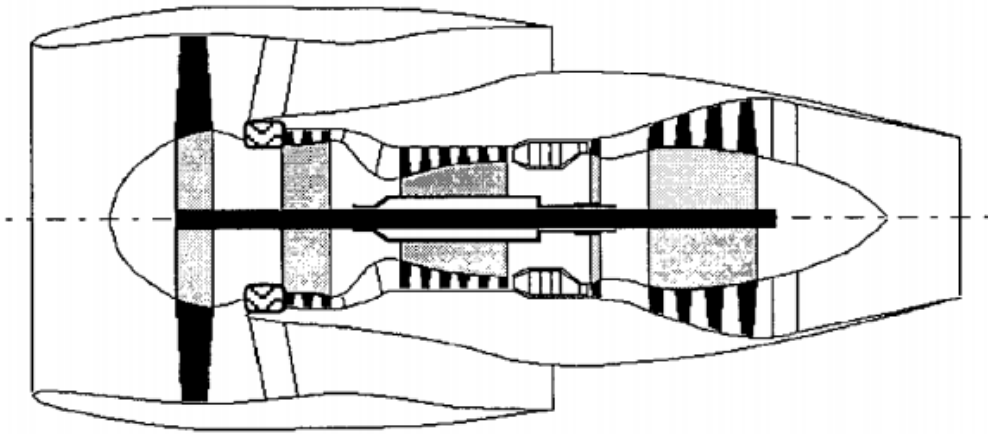

Figure 2.12: Referenced engine used by Boggia [32]

2.9.1.1 Precooled engine (core)

The precooled unconventional engine in theory consists in cooling down the core inlet air flow using liquid hydrogen. To achieve this, the liquid hydrogen is vaporized after passing through a heat exchanger located inside the inlet guide vanes.

The lower inlet temperature (before the compressor) allows one to design the engine with a relatively higher pressure ratio without increasing the temperature at the exit of the compressor, thus improving both the performance of the engine and it's life.

In order to achieve a satisfying heat flux and to fulfill safety requirements, according to Boggia [32], the upstream vanes of the compressor, need to have it's chord doubled.

2.9.1.2 Elevated TET engine

For the typical conventional engines, there is a cooling bleed taken at the compressor which is then used to cool down the nozzle guide vanes (NGVs) and the blades of the high pressure turbine. Due to this cool air bleed, the high pressure turbine can operate at temperatures 15% above the maximum allowable metal temperature.

After being pre-heated and vaporized, hydrogen can provide a much cooler bleed and thus, increase the turbine inlet temperature significantly without exceeding the maximum allowable temperature of NGV's and turbine blades.

2.9.1.3 Pre-heated fuel engine

The pre-heating of the fuel before combustion has quite a positive impact in the fuel consumption (reduces fuel consumption) since a temperature increase in the hydrogen fuel translates into an increased energy content in the fuel, in other words, this way more energy that is stored in the fuel can be used, otherwise this energy would be lost.

Given the previous fuel treatment, less fuel is used in order to achieve a similar thrust level of an engine without pre-heating (reference engine).

2.9.2 Combustion chamber

The combustion of hydrogen is more complex than just adjusting the fuel-to-air ratio. The geometry of the combustion chamber is in fact the factor that mostly contributes to the efficiency of hydrogen fuel combustion, for instance, hydrogen fuel combustion in a conventional combustion chamber has inferior results to conventional fuels. This inferior results can be explained due to an inefficient mix of hydrogen fuel and air which prompts the formation of diffusive flames, where stoichiometric ratios are created around the flame leading to high temperature and the inherent formation of NO_x species [3].

Two combustion chamber concepts were developed in order to tackle critical aspects such as combustion efficiency, flame stability and acoustics. These concepts are the Lean Direct Injection (LDI) and Micro-mix. Both concepts are focused on reducing flashback and increasing the mixing of fuel and air. LDI and Micro-mix are successful in promoting a better fuel mix, which diminishes the flame length by enabling a completed combustion sooner, leading to smaller residence times. Since NO_x emissions are dependant on residence times and temperature, improving such aspects results in a decrease of NO_x emissions [3].

2.10 Auxiliary power unit (APU)

APUs represent an important source of air pollutant emissions at main airports, depending on how much they are used [36]. As such, implementing LH_2 fuelled APUs could present a significant improvement regarding aircraft emissions on the ground and as a whole.

Most of the APU's systems and configuration can remain unchanged. However, a few components have to be re-designed in order to accommodate LH_2 [26]. A new heat exchanger needs to be developed in order to pre-heat the LH_2 before it enters the combustion chamber, thus enabling a more stable combustion process. The fuel control unit (FCU) present in conventional APUs is to be replace by a Hydrogen Fuel Control Unit (HFCU) in order to provide control and metering of hydrogen. The combustion section of the APU would have to endure many modifications in order to reduce NO_x emissions and to ensure stable operation on the whole power range [26].

Chapter 3

Design requirements

Conceptual aircraft design typically starts with a vast array of design requirements which are established either by the prospective customer or as a company-generated guess as to what future customers may need [37].

More specifically, it can be said that the sizing of an aircraft is the process of finding a constrained balance between size, thrust and energy requirements of an aircraft under the objective of fulfilling all its transport tasks specified in the aircraft top-level requirements (ATLRS) and of the compliance with the airworthiness regulations [38]. Also according to Pornet [38] there are three major categories of requirements that can be highlighted when the goal is to size and evaluate the performance of an aircraft.

The first major category are the performance requirement constraints, these requirements relate the thrust of an aircraft to it's size in order to fulfill point performance requirements.

The second category of requirements englobes the mission requirements which relate the amount of energy to the size of the aircraft in order to transport a design payload along a specified design mission.

The last category represents the requirements and constraints regarding the the manufacturing and operating costs of the said aircraft. These kind of requirements are heavily influenced by the need of the industry to produce a competitive product.

In order to better illustrate the purposes of this master thesis, it will be taken a closer look on the mission requirements. According to Corke [39] the mission requirements specify many performance aspects, some of these performance aspects are instrumental to the development of the present thesis and they are the following.

- The aircraft purpose or mission profile
- The type(s) and amount of payload
- The cruise and maximum speeds
- The range or radius with normal payload
- The endurance

Given the importance of the items presented above, some time must be spent explaining them individually and contextualizing, when possible, with the spectre of the work being developed here. Figure 3.1 illustrates the typical design flow of traditional aircraft sizing.

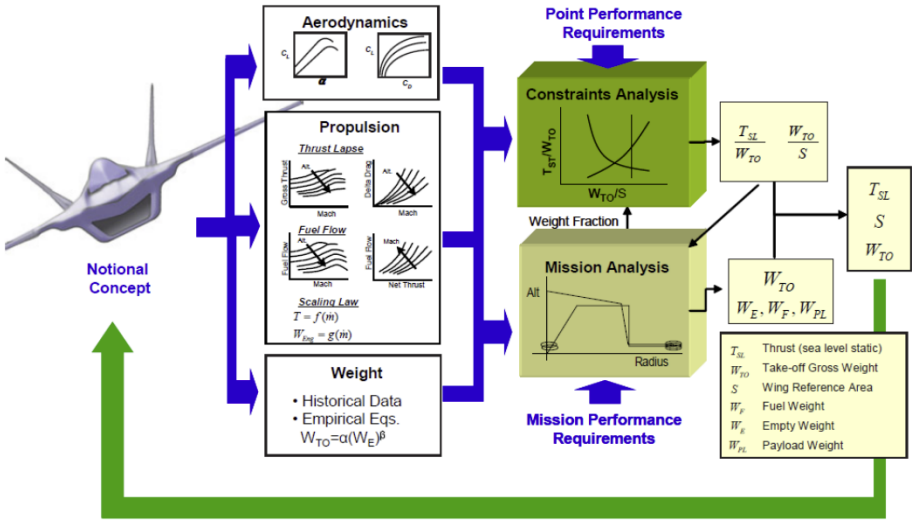

Figure 3.1: Traditional aircraft sizing according to Mattingly [40].

3.1 Mission requirements and performance aspects

3.1.1 Aircraft purpose

The starting point for any new aircraft is to clearly identify its purpose. First of all, one must must know if the aircraft to be designed is envisioned to be a commercial aircraft, a cargo aircraft or a military aircraft (which may further diverge into different modes of operation). Having chosen from one of the three categories described above, one can further filter down the purpose of the designing aircraft with respect to it's range, payload, cruise speed and more [39]. As for the present thesis, there is no doubt that the aircraft is intended to be a commercial aircraft where the range and cruise speed are essential to keep this LH_2 passenger aircraft competitive in the commercial aircraft demanding market.

3.1.2 Types and amount of payload

There are three types of payload. These payload types are passengers, cargo and ordnance. The latter is a type of payload typically found on military aircraft and it is considered expendable since sometime during the course of the flight this payload is dropped and the aircraft finishes the rest of the mission without this piece of payload. Examples of this kind of payload are devices such as bombs, missiles and ammunition for armament within the aircraft. The passengers and cargo are considered non-expendable payloads given that they are expected to stay within the aircraft for the whole duration of the flight. It is also important to note that for commercial aircraft the pilots and cabin crew are not considered part of the payload as opposed to small general aviation whose cabin crew and pilots are considered as

payload [39].

3.1.3 Cruise and maximum speeds

The mission of an aircraft usually dictates its speed and range. In the particular case of commercial aircraft powered by jet engines the typical interval for cruise speed is set around 0.785 Mach. This range of cruise speeds is close to optimum for maximizing the combination of payload weight, range, and speed [39].

3.1.4 Range with expected payload

The range of an aircraft can be simply defined as the furthest distance an aircraft can fly without having to stop to refuel or, in the case of military aircraft, not needing to refuel during plain flight. The designer must be specially meticulous when choosing the range of the aircraft since, according to experimental data, it has an exponential increasing effect on the Maximum Take-off Weight (MTOW) of the aircraft. To sum it, a high MTOW will most likely render the aircraft noncompetitive compared to the market needs and the costs implied with high take off weights [37].

3.1.5 Endurance

As the name may suggest, Endurance stands for the amount of time an aircraft can remain on the air with its engines running (be careful not to confuse with the furthest distance as said in the previous subsection). As stated by Corke [39], for a commercial aircraft, the flight plan must include an endurance phase in order to allow for any time that might be spent in a holding pattern prior to landing. Note that for international operation the required holding time is no less than 30 minutes.

Chapter 4

Implementation

In order to develop a new concept aircraft fuelled by LH_2 that is compatible with the actual aeronautical market, demands and the technologies available to present day, a practical and realistic strategy must be devised. A possible strategy is to take the characteristics of a widely used and proven commercial aircraft to serve as the basis for the conceptual design, a basis from which many alterations will be performed upon so that one can achieve a feasible design that is compatible with the constraints that are imposed by the switch from a kerosene fuelled aircraft to a conceptual aircraft fuelled by LH_2. The aircraft chosen as the basis for all the analytical models yet to be presented on this chapter is the Boeing 737 - 800 since it is used all over the world for many years, earning a strong positive reputation given its reliability and safety [41]. Such qualities are undeniably a good basis from which to improve and redesign.

4.1 Reference aircraft

This section is dedicated to the reference aircraft since, as it has been stated at the beginning of the chapter, it plays a critical role in the development of the strategy implemented to design the conceptual LH_2 aircraft. The chosen aircraft is the Boeing 737 - 800 not only due to it's reliability and safety reputation, but also given the type of mission it carries out and consequently, the range for which it is designed (short to medium haul flights).

Figure 4.1: Reference aircraft - Boeing 737-800 [42].

Knowing that one of the main focus of this master thesis is to study the environmental and human health impacts resulting from the implementation of a LH_2 fuelled aircraft that operates at the short to medium haul ranges, the Boeing 737 - 800 is the ideal candidate to set as a starting point.

Table 4.1 summarizes some very important aspects and technical specifications of the Boeing 737 - 800 that are essential to provide the MATLAB scripts with some baseline properties and thus allow for the initialization of the iterative process leading to the creation of a robust LH_2 conceptual aircraft.

Table 4.1: Technical specifications for Boeing 737 - 800 Winglets [43] [44] [45] [46].

Property	Symbol	Measuring unit (SI)	value
Mass and other properties			
Fuselage Length	$L_{fuselage}$	m	38.08
Fuselage diameter	$\phi_{fuselage}$	m	3.76
Maximum Take-off Weight	W_{TO}	Kg	79016
Operating Empty Weight	W_{empty}	Kg	41413
Maximum Zero Fuel Weight	W_{MZF}	Kg	62732
Range With Maximum Payload	R	m	$4.074 \cdot 10^6$
Maximum Payload	P	Kg	21587
Conditions during cruise			
Mach number	M_{cruise}	-	0.785
Velocity	V_{cruise}	m/s	231.89
Altitude	h_{cruise}	m	10668
Specific Fuel Consumption	SFC_{cruise}	$Kg/W \cdot s$	0.635
Lift-to-Drag ratio	$\left[\frac{L}{D}\right]_{cruise}$	-	17.26
Conditions during loiter			
Stall Speed	S_{loiter}	m/s	77.17
Endurance	E_{loiter}	s	1800
Specific Fuel Consumption	SFC_{loiter}	$Kg/W \cdot s$	0.5
Lift-to-Drag ratio	$\left[\frac{L}{D}\right]_{loiter}$	-	19.93

4.2 Mission requirements

The following mission profile was chosen for the conceptual LH_2 aircraft mainly for it's ability to simulate most phases of an aircraft's flight and also for it's ability to provide a solid basis for comparisons with other aircraft, some of which propelled by alternative fuels.

The mission profile is crucial for the sizing of the conceptual LH_2 aircraft and since there is great interest in replicating the operating capabilities and ranges of the selected reference aircraft (Boeing 737 - 800), both cruising and loiter top-level requirements presented in table 4.1 are reapplied to this mission (altitude, cruise mach number and loiter endurance time). Below can be found a schematic of the mission profile envisioned for the LH_2 aircraft (figure 4.2)

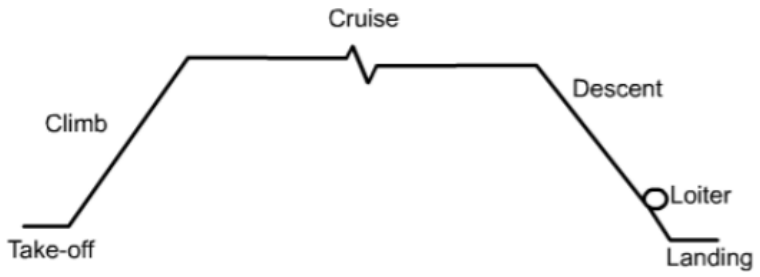

Figure 4.2: Mission profile to be carried out by the conceptual LH_2 aircraft [47].

4.3 Hydrogen tanks modelling

The storage of LH_2 at cryogenic temperatures on the aircraft constitutes the biggest challenges for the widespread use of LH_2 fuelled aircraft and due to this fact, special attention has to be payed to the designing of tanks capable of storing hydrogen at cryogenic temperatures and preventing any risks of catastrophic failure [7]. The modelling of the LH_2 tanks is of capital importance for the scope of this thesis, since the dry mass of these tanks will have a major impact on the MTOW of the conceptual hydrogen aircraft being designed.

In order to model the hydrogen tanks a MATLAB code has been developed to allow for the calculation of the dry mass of the tank, the time before venting and the heat flowing across the layers of the tank. The three parameters listed before are essential for the development and design of such unconventional aircraft

The diameter of the tank is assumed to be constrained by the diameter of the aircraft that has been chosen as the basis for the development of this study and thus, represents an input for the MATLAB script in question. The insulation type and thickness is also another input to this script, however, this input is mostly influenced by the literature and previous conclusions about this subject and strongly related to the thermal branch of the design project. There are two more inputs for this script which are closely related to the mechanical design aspect of the problem, these will be the venting pressure and the filling pressure. These two last parameters, in order to be fully understood by the reader, imply some knowledge about tanks in general and more particularly LH_2 tanks and for this reason, these parameters will be explained during this section. For the sake of clarity, table 4.2 resumes the inputs presented above that are inherently needed for this script.

Table 4.2: Matlab script input parameters.

Input	Measuring unit (SI)
Fuselage diameter	m
Insulation type	-
Insulation thickness	m
Venting pressure	Pa
Filling pressure	Pa

A direct consequence from the flight of the aircraft or even holding out periods on the ground, is the inevitability of heat leaking through all the insulation of the tank. The heat flow towards the interior

of the tank will cause an increase in temperature of the LH_2, as a result of the temperature increase, the LH_2 gradually turns into GH_2 (this process is known as boil-off and was mentioned in chapter 2). The increasing quantities of GH_2 will induce an increase of pressure inside the tank. The pressure will keep increasing until the maximum allowed pressure of the tank (a design parameter) is reached. The maximum allowed pressure is no more and no less than the venting pressure mentioned above. Venting is a procedure that consists in the release of GH_2 from the inside of the tank to the exterior, this action is essential to keep the pressure inside the tank below or equal to the maximum allowed pressure and thus preventing the tank from catastrophic failure [7].

As it is stated by Christopher Winnefeld et al. [9], if one assumes that it is LH_2 being vented, the mass that needs to be vented is much greater than it would be if it was GH_2 being vented to the exterior in order to achieve the same pressure drop. All considered, it would be good practice to have both liquid and gaseous hydrogen inside the tank should the need to vent arise. Around 3% of the volume of the tank should be filled with GH_2, which translates to a fill level of $y_{fill} = 0.97$. However, bear in mind that the value y_{fill} is dependant on the values chosen for the venting pressure and the filling pressure since these two will influence the mean density of the LH_2. To better illustrate the phenomenon described before, if a value of 2 bar is prescribed for the venting pressure and the filling pressure is equal to 1 bar, this conjugation of both pressures will impose a fill level equal to 0.92 ($y_{fill} = 0.92$) [9].

Although complex, it is possible to predict and control the pressure fluctuations inside the tank, which, as it has been stated previously, are a consequence of the heat leaking through the insulation of the tank.

A mathematical model has been proposed by Lin et al. [48]. This mathematical model is built around the first law of thermodynamics and the principle of conservation of mass and is given, under some assumptions and simplifications (elasticity of the tank is neglected, there is no incoming mass flow rate and work input is null), by the following equation:

$$\frac{dp}{dt} = \frac{1}{V_t}\left[\rho\left(\frac{\partial u}{\partial p}\right)_p\right]^{-1}\left[\dot{Q} - \dot{m}_{out}\Delta h_v(x+\rho^*)\right] \tag{4.1}$$

Where ρ^* represents the density ratio and is defined as:

$$\rho^* = \frac{\rho_g}{\rho_g - \rho_l} \tag{4.2}$$

And most importantly,

$$\phi = \left[\rho\left(\frac{\partial u}{\partial p}\right)_p\right]^{-1} \tag{4.3}$$

The variable ϕ on equation 4.3 represents a crucial term present on equation 4.1 called energy derivative. The energy derivative can be calculated with the aid of the thermodynamic data available at National Institute of Standards and Technology's database (NIST) [7]. Figure 4.3 displays the energy derivative in function of the average density inside the tank for different pressures.

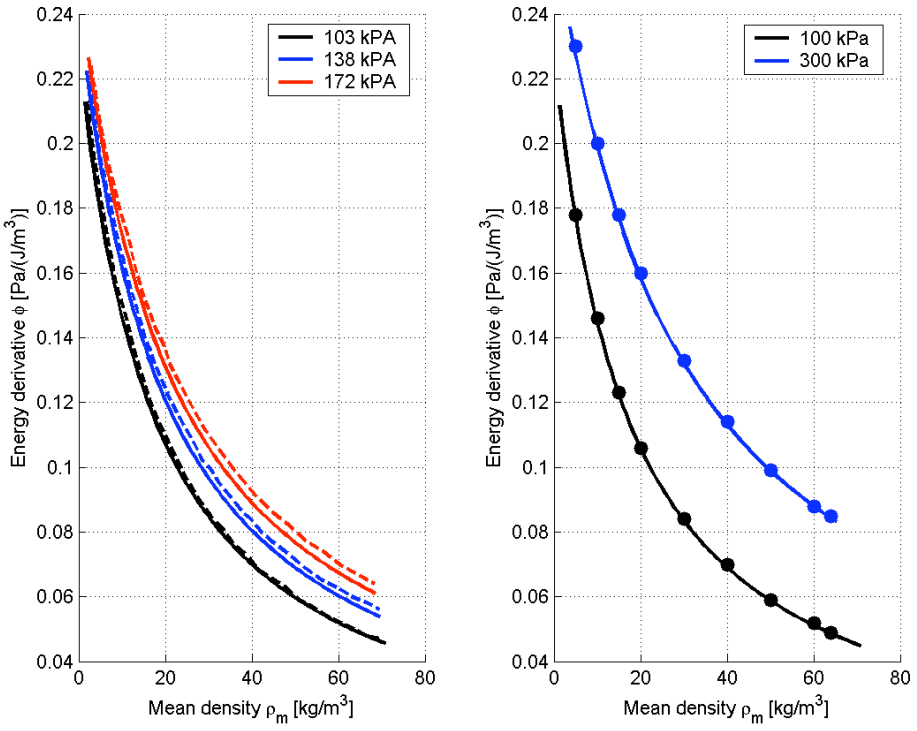

Figure 4.3: Energy derivative as a function of pressure and average density, adapted from Verstraete [7].

4.3.1 Tank mechanical design

As mentioned in chapter 2, only integral tanks are considered in the ambit of this dissertation. The use of integral tanks imply that this component must be reliable and resistant enough to deal with all the stresses that the aircraft, particularly it´s fuselage, are submitted to. Examples of these stresses are, for instance, bending loads on the fuselage, aerodynamic loads, dynamic loads prompted by gusts, accelerations felt by the aircraft and vibrations. Concerning the interior of the tanks, sloshing of the fuel is expected as it is consumed during the flight and the inherent pressure differential between the outside of the tank and the inside of the tank [7].

Most of the loads described before can only be determined accurately with the help of a strong finite element analysis (FEM) and thus be able to fully design the tank to cope with all the loads applied to it. However, a detailed FEM analysis goes well beyond the scope of this thesis and as such, the analytical model of the tank design will be primarily based on the pressurization loads and then a safety factor is added to account for other stresses, as Verstraete suggests [7].

The geometry of the tanks needs to be selected upfront since all the posterior calculations for the conceptual LH_2 aircraft will be somewhat influenced by the geometry of the tank. Below a schematic (figure 4.4) is presented that represents the general geometry for cryogenic tanks and what design parameters can be change in order to obtain a different geometry. A table (table 4.4) presenting the values concerning p_{vent} and p_{fill} is also presented.

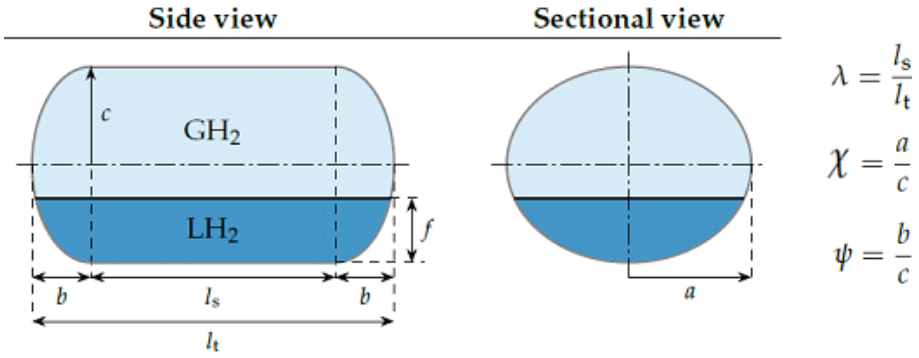

Figure 4.4: Tank geometry parameters, adapted from Christopher Winnefeld et al. [9].

Table 4.3: Geometry parameters observations.

Adimensionalised parameters	Value	Observations
λ	-	Dependant of fuel fractions
χ	1.0	Restricted by diameter of the reference aircraft
ψ	1.0	Selected for this thesis

Table 4.4: Selected values for venting and filling pressures.

Design pressure input	Selected pressure value (Pa)
Venting pressure	3.5×10^5
Filling pressure	1.2×10^5

The values for the venting and filling pressures (table 4.4) have been selected based on the conclusions taken from the cryoplane project, which has similar goals to the ones presented in the ambit of this master thesis and thus it makes perfect sense to make use of the resulting data from the cryoplane project.

Having established the geometry and shape of the tank (table 4.3), one can now select the right methods and expressions to calculate the thickness of the tank walls. The selected material for the tank walls is aluminium alloy 2219 since it gathers all the requirements described in chapter 2. This alloy possesses a density of 2825 Kg/m^3 and an allowable stress of 172.4 MPa [9]. Verstraete [7] suggests using the following expression based on the ASME Boiler and pressure vessel method:

$$t_w = \frac{p_{des} \cdot d_{int}}{2\sigma_a \cdot e_w + 0.8 p_{des}} \tag{4.4}$$

The thickness of the tank cylindrical shell (or wall) is represented by t_w, p_{des} stands for the venting pressure, σ_a represents the allowable stress for the tank material, the diameter of the interior of the tank is represented by d_{int} and finally, e_w stands for the efficiency of the weld and has a value of 0.8 (e_w = 0.8) [9].

For the bulkheads, it is necessary to use another formula given their spherical shape. As it is stated for ASME torispherical heads, the thickness of the bulkheads can be calculated applying the following expression:

$$t_{bulkheads} = \frac{p_{des} \cdot d_{int} \cdot K}{2\sigma_a \cdot e_w + 2p_{des} \cdot (K - 0.1)} \tag{4.5}$$

Where K is given by the general expression for elliptical bulkheads [7]:

$$K = \frac{1}{6}\left[2 + \psi\right] \tag{4.6}$$

As it is indicated in table 4.3, the ratio ψ is equal to one, and as such, the bulkheads will have a spherical shape. Thus, the tanks will be comprised of two simple elemental shapes, a cylinder shape of length unknown and two semi-spheres, each placed at both ends of the main cylinder. The length of the cylinder shaped section of the tank is an unknown which is dependant on the amount of LH_2 fuel that the conceptual LH_2 fuelled aircraft requires in order to perform the selected mission profile presented in section 4.2. The length of the cylinder shaped section of the tank will have a direct impact on the designing of the conceptual LH_2 fuelled aircraft being developed in this thesis. This statement will be analyzed with great detail in the following sections of this thesis since it is of capital importance in this work.

4.3.2 Tank thermal design

The thermal design is absolutely crucial in order to design an effective cryogenic tank, especially for the aeronautic industry, since the aircraft needs to be as light as possible, yet, one cannot afford to decrease the insulation (making the said aircraft less heavy) to the point where the heat flowing inside the tank is so elevated that enormous quantities of GH_2 have to vented, so that the pressure inside the tank is kept at the designed pressure.

There are different materials that can be used to insulate the LH_2 tanks as it has been stated in chapter 2. However, according to Verstraete [49], although the MLI has a lower thermal conductivity than foams, the fact that MLI insulation implies the use of a double metal tank wall in order to maintain the vacuum this type of insulation requires renders the tank inevitably heavier than it would be if foam was used as the insulation material. Another disadvantage of using MLI as insulation instead of foam, is it's degradation of thermal insulation performance with the passing of time provoked by the loss of vacuum. The loss of vacuum and, consequently, the decrease of thermal insulation performance represents a major safety issue since catastrophic failure may occur. The cost of using MLI as the selected material for the insulation of the LH_2 tank is also significantly higher than the it´s counterpart.

Given the arguments presented above, especially those regarding safety and weight, the thermal model developed in this thesis will contemplate only the use of foam as an insulation material. Rohacell foam has been selected. The thickness of the insulation layer, a design parameter (as stated earlier), and Rohacell foam properties can be found in table 4.5:

Table 4.5: Foam layer thickness and physical properties of Rohacell foam, values retrieved from [9] and [49].

Property	Symbol	Unit	Value
Density	ρ	Kg/m^3	35.24
Thermal conductivity	K	W/mK	5×10^{-3}
Insulation layer thickness	t_{foam}	m	0.119

The thickness of the insulation layer was selected according to the findings of Verstraete et al. [49] assuming a single tank configuration.

4.3.2.1 Thermal resistance of mixed LH_2 and GH_2 by convection inside the tank

For the reasons mentioned in the beginning of this chapter, there must always be present a mixture of both LH_2 and GH_2. Due to the mixture of LH_2 and GH_2 inside the tank, convective forces will be present, and to address this issue, different correlations must be considered in order to account for the different physical states of the hydrogen.

Liquid phase

According to Daney et al. [50], the following correlation enables one to obtain the Nusselt number for the liquid phase convection:

$$Nu = 0.104 \cdot Ra^{0.352} \tag{4.7}$$

Where Ra (Rayleigh number) is set between the range of $7 \times 10^8 < Ra < 6 \times 10^{11}$ and Nu represents the Nusselt number.

After obtaining the Nusselt number, it is possible to compute the convective heat transfer coefficient for LH_2, employing the following expression:

$$h_{LH_2} = \frac{Nu \cdot K_{LH_2}}{l_s} \tag{4.8}$$

Where h_{LH_2} is the convective heat transfer coefficient for LH_2, Nu is the Nusselt number calculated for liquid state hydrogen and K_{LH_2} is the thermal conductivity of LH_2.

Gaseous phase

For the gaseous phase convection, Verstraete [7] suggests applying the following value for the Nusselt number:

$$Nu = 17 \tag{4.9}$$

Using the value of Nusselt number selected for GH_2, it is possible to compute the convective heat transfer coefficient for GH_2, employing the following expression:

$$h_{GH_2} = \frac{Nu \cdot K_{GH_2}}{l_s} \tag{4.10}$$

Where h_{GH_2} is the convective heat transfer coefficient for GH_2, Nu is the Nusselt number calculated for gaseous state hydrogen and K_{GH_2} is the thermal conductivity of GH_2.

Full internal convection

With the Nusselt number for both phases, one can easily calculate the convective heat transfer coefficient for each phase (liquid and gaseous). After obtaining the convective heat transfer coefficient for each phase, the overall heat transfer coefficient can be obtained by the following expression [9]:

$$h_{internal} = \frac{1}{S_w} \cdot (h_{LH_2} S_{LH_2} + h_{LH_2} S_{GH_2}) \tag{4.11}$$

Where S_{LH_2} and S_{GH_2} are the wetted areas of LH_2 and GH_2 respectfully, h_{LH_2} is the convective heat transfer coefficient for LH_2 and finally, h_{GH_2} stands for the convective heat transfer coefficient for the GH_2.

Taking into consideration the geometry of the tank and the previous result, one is now able to apply the thermal resistance analogy, translating into the following result [7]:

$$R_{internal} = \frac{1}{2 \cdot \pi \cdot r_{int} \cdot l_s} \cdot \frac{S_w}{h_{LH_2} S_{LH_2} + h_{LH_2} S_{GH_2}} \tag{4.12}$$

4.3.2.2 Thermal resistance of tank metal wall

The study of the heat flux along the tank metal wall is a simple conduction heat transfer problem with cylindrical coordinates, and as such, according to Incropera et al. [51], the thermal resistance is given by:

$$R_{wall} = \frac{1}{2 \cdot \pi \cdot r_{int} \cdot l_s} \cdot \frac{\ln\left(\frac{r_w}{r_{int}}\right)}{K_{Al}} \tag{4.13}$$

Where r_{int} is the inner radius of the tank and r_w represents the outer radius of the tank, or in other words, the r_w is simply the sum of the inner radius of the tank and the thickness of the tank wall, which has been calculated previously at the mechanical design phase. The thermal conductivity of the metal is hereby expressed as K_{al}.

4.3.2.3 Thermal resistance of the of the insulation foam

Similarly to the previous section, the computation of the thermal resistance of the insulating foam is also a conduction heat transfer problem with cylindrical coordinates, and thus, the same expression from Incropera et al. [51] can be applied once again:

$$R_{insulation} = \frac{1}{2 \cdot \pi \cdot r_w \cdot l_s} \cdot \frac{\ln\left(\frac{r_{ins}}{r_w}\right)}{K_{foam}} \tag{4.14}$$

With r_{ins} representing the outer radius of the insulation, more specifically, r_{ins} is the sum of the internal radius (r_i), the tank wall thickness and lastly, the thickness of the insulating foam. The thermal conductivity of the foam is hereby expressed as K_{foam}.

4.3.2.4 Thermal resistance of aircraft skin

The computation of the thermal resistance of the aircraft skin is, as seen before, also a conduction heat transfer problem with cylindrical coordinates and consequently, the expression provided by Incropera et al. [51] can be once gain applied to solve this problem:

$$R_{skin} = \frac{1}{2 \cdot \pi \cdot r_{ins} \cdot l_s} \cdot \frac{\ln\left(\frac{r_{skin}}{r_{ins}}\right)}{K_{skin}} \tag{4.15}$$

Where r_{skin} is the radius of the aircraft's fuselage, r_{ins} has been defined in the previous section and finally, K_{skin}, is the thermal conductivity of the composite material which serves as the aircraft skin.

4.3.2.5 Thermal resistance of the involving atmosphere

Whether the aircraft is flying or simply stationary on the ground (hold out period), forced convection will most likely be present. According to Verstraete [7], there is no correlation for the phenomena of forced convection along the axis of a cylinder, and due to this matter, a flat plate correlation (Buchlin) must be adopted:

$$Nu = 0.03625 \cdot Pr^{0.43} \cdot Re^{0.8} \tag{4.16}$$

Where Re is the Reynolds number and Pr stands for the Prandtl number. After computing the Nusselt number using equation 4.16, the external convective heat transfer coefficient can be obtained by the following relation:

$$h_{exterior} = \frac{Nu \cdot K_{air}}{L} \tag{4.17}$$

With K_{air} representing the thermal conductivity of the air and L being the length of the flat plate, which in this model is the length of the cylinder, l_s.

In order to be able to solve equation 4.16 the Prandtl and Reynolds numbers must be computed first.

The Prandtl number is defined here as:

$$Pr = \frac{\mu_{air} \cdot c_p}{K_{air}} \tag{4.18}$$

Where μ_{air} represents the viscosity of the air.

The following expression enables one to compute the Reynolds number, where ν is the flight velocity:

$$Re = \frac{\nu \cdot \rho_{air} \cdot L}{K_{air}} \tag{4.19}$$

It is now possible to compute the Nusselt number through equation 4.16 and then, having solved the Nusselt number, one can compute the external convective heat transfer coefficient ($h_{exterior}$) using equation (4.17).

Apart from the heat being transferred by convective mechanisms, radiation also plays a considerable part in order to fully determine the total external heat transfer coefficient for the aircraft skin. According to Verstraete [7], it is possible to obtain an equivalent convective coefficient to account for the heat being transferred by radiation, the equation below illustrates clearly this result:

$$h_{radiation} = \sigma \cdot \epsilon \cdot (T_{skin}^2 + T_{\infty}^2) \cdot (T_{skin} + T_{\infty}) \tag{4.20}$$

Where T_{skin} and T_{∞} represent the temperature of the aircraft and the temperature of the flow respectively. σ is the Stefan-Boltzmann constant, ϵ stands for the emittance of the surface of the aircraft skin having the value of 0.95 (ϵ = 0.95) been assumed since most aircraft are painted white.

Now that both the external convective heat transfer coefficient ($h_{exterior}$) and the equivalent convective coefficient for the radiation on the aircraft skin ($h_{radiation}$) can be computed, it is possible to compute the total external heat transfer coefficient for the aircraft skin:

$$h_{total} = h_{exterior} + h_{radiation} \tag{4.21}$$

Thus, the thermal resistance that represents the total external heat transfer can be expressed by the following equation:

$$R_{external} = \frac{1}{2 \cdot \pi \cdot r_{fuselage} \cdot l_s} \cdot \frac{1}{h_{total}} \tag{4.22}$$

4.3.3 Heat flux calculation

So far, it has exclusively been taken into account the heat transfer through the insulation of the tank, however, there is certainly going to be heat flowing into the tank through the piping system and the connections of the tank (thermal bridges). This phenomena can be accounted for by imposing a margin of 30% of surplus heat input, as it is suggested by Verstraete [7].

Equation 4.23 enables one to compute the heat flux rate flowing across each one of the layers that comprise the LH_2 tanks:

$$\begin{bmatrix} -1 & 1 & 0 & 0 & 0 & 0 \\ 0 & -1 & 1 & 0 & 0 & 0 \\ 0 & 0 & -1 & 1 & 0 & 0 \\ 0 & 0 & 0 & -1 & 1 & 0 \\ 0 & 0 & 0 & 0 & -1 & 1 \end{bmatrix} \cdot \begin{bmatrix} T_{LH_2} \\ T_w \\ T_{ins} \\ T_{ins-outer} \\ T_{skin} \\ T_{\infty} \end{bmatrix} - \begin{bmatrix} R_{inside} \\ R_w \\ R_{ins} \\ R_{skin} \\ R_{\infty} \end{bmatrix} \cdot \frac{\dot{Q}}{1.30} = 0 \tag{4.23}$$

Having calculated the heat flux ($\dot{Q}$) and looking back at equation 4.1 it is possible to calculate the venting time assuming that there is no mass flowing out of the hydrogen tank ($\dot{m}_{out} = 0$).

4.3.4 LH_2 tanks dry mass

Ultimately, after the mechanical and thermal design of the tank are completed and in order to be able to size the conceptual LH_2 aircraft's mass, one must calculate the dry mass of the tank. Since all material densities and thicknesses are now known, the dry mass of the hydrogen tank can be calculated using the following expression:

$$W_{tank} = \sum_{layer=1}^{3} V_{layer} \cdot \rho_{layer} \cdot L_{layer} \tag{4.24}$$

4.4 Aircraft conceptual design strategy

The LH_2 tanks are the most crucial element in the design of the conceptual LH_2 aircraft. Given the results obtained in the previous section it is now possible to calculate the dry mass of the tank. However, the total length of the tank is still unknown. To tackle this issue (please revisit figure 4.4 for a better understanding of the problem), the length of the cylindrical section of the tank, l_s, will be fixed as one meter (l_s = 1 meter) and both remaining semi-spheres are maintained fixed according to the parameters already shown on table 4.3 which are constricted by the diameter of the fuselage of the reference aircraft (3.76 meters). The assumption of the unitary length of the cylindrical section of the tank enables one to initiate the iterative process of sizing the LH_2 aircraft which will ultimately lead to the calculation of both the total length of the LH_2 tank and the very essential MTOW.

The following image (figure 4.5) is an internal schematic of the Russian aircraft Tupolev tu-155 where it is possible to locate the positioning of the LH_2 tank inside the aircraft's fuselage.

Similarly to the aircraft presented in figure 4.5, the LH_2 tanks of the conceptual hydrogen aircraft will also be placed in a location within the fuselage (after the aft pressure bulkhead) where the cross section area is constant. This assumption is crucial in the development of the strategy based on which the conceptual LH_2 aircraft will be built. The cross sectional area needs to be constant along the axis of the fuselage in order to accommodate the geometry previously defined for the tank.

The length of the tank, as said before, is an iterative variable. As a starting point for the strategy used to build the conceptual LH_2 aircraft, the length of the reference aircraft will be used as a starting point. To describe the process in a simple way, the total length of the tanks, l_t, needed to perform the mission is added to the length of the reference aircraft ($L_{Ref'A/C}$) resulting in the total length of the LH_2 conceptual aircraft ($L_{LH_2'A/C}$).

4.4.1 Aircraft Sizing

Having the mission already been defined and the general design of the aircraft proposed, the next logical step is to calculate the MTOW. In order to calculate the MTOW, the method devised by Corke [39] will

(a) Tupolev tu-155 three dimensional view [52]

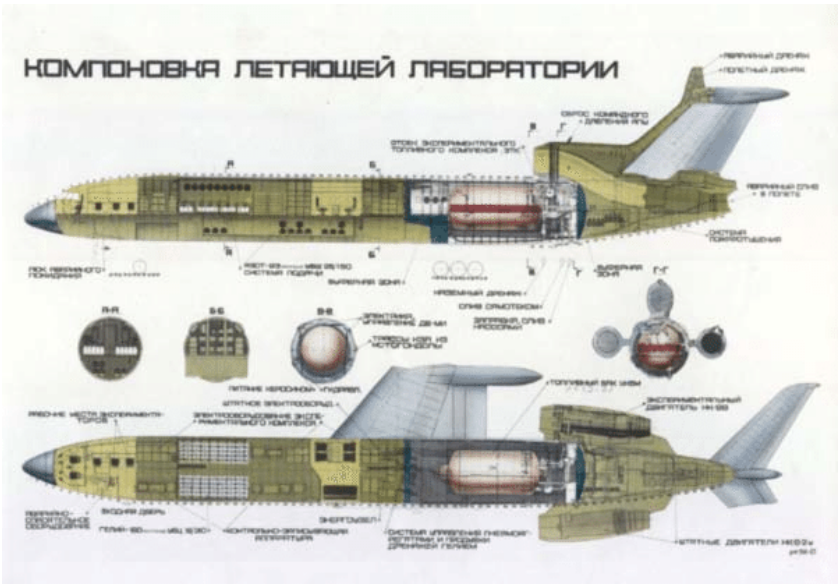

(b) Tupolev tu-155 schematic detailed view [53]

Figure 4.5: Positioning of the hydrogen tanks inside the Russian aircraft Tupolev tu-155

be the backbone of this analysis.

The MTOW of the LH_2 conceptual aircraft is divided into the following sub components:

$$W_{TO} = W_{fuel} + W_{payload} + W_{empty} \tag{4.25}$$

The payload can be further divided into either nonexpendable or expendable payload:

$$W_{payload} = W_{nonexpendable} + W_{expendable} \tag{4.26}$$

However, for this conceptual aircraft, as said in previous sections, there is no expendable payload since it is a commercial aircraft. Focusing on the nonexpendable weight component, it is comprised of the weight of the passengers, crew and an extra weight to account for luggage and other objects. The number of passengers for the conceptual aircraft is the same as the reference aircraft and the parcel

related to the weight of the luggage and other objects has been fixed as the same for both aircraft.

Regarding the empty weight, in order to obtain the empty weight of the conceptual LH_2 aircraft, excluding the dry weight of the LH_2 fuel tanks, a 6% increase in mass must be applied to the fuselage of the reference aircraft to account for the structure responsible for attaching the LH_2 tank to the said fuselage [54]. The absence of fuel (Kerosene) on the wings also imposes a mass increase of 6% on top of the total wing mass of the reference aircraft. The mass of the wing needs to be increased since the mass of the kerosene fuel present on the aircraft wings promotes a lower bending moment on the wing, meaning that for the conceptual aircraft's case, in order keep the the bending moment on the wing to safe values, extra mass needs to be added [54].

Given the considerations presented above, it is necessary to know the weight of both the wings and the fuselage of the reference aircraft and then apply the necessary increases in weight for both these structures, thus obtaining the total empty weight of the conceptual LH_2 aircraft excluding the fuel tanks. The following chart (figure 4.6) provided by MIT gives some estimates regarding fractional weight breakdown for commercial aircraft.

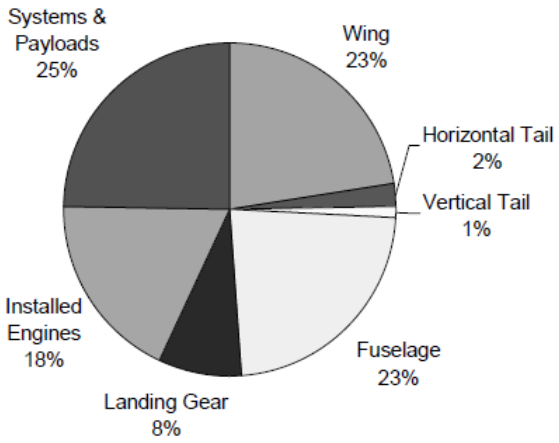

Figure 4.6: Estimated operating empty weight fraction breakdown for the typical commercial aircraft [55].

Cross checking the estimated empty weight fraction breakdown from figure 4.6 and the percentages of mass that need to be increased into specific aircraft modules will result in the following expression:

$$W_{\mathrm{LH_2}'A/C-empty-notanks} = 0.06 \cdot 0.23 \cdot W_{Ref'A/C-empty} + 0.06 \cdot 0.23 \cdot W_{Ref'A/C-empty} \tag{4.27}$$

Where $W_{\mathrm{LH_2}'A/C-empty-notanks}$ is the empty weight of the conceptual LH_2 aircraft without accounting for the hydrogen tanks and $W_{Ref'A/C-empty}$ stands for the empty weight of the reference aircraft.

4.4.1.1 Fuel fraction estimates

This approach consists in determining the quantity of fuel burnt in each flight phase of the mission presented in section 4.2.

For any given mission segment k, the mission's segment weight fraction is expressed the following way:

$$W_{Segment-k} = \left[\frac{W_k}{W_{k-1}}\right] \tag{4.28}$$

Table 4.6 summarizes the fuel weight fraction for every segment k of the mission according to Corke [39].

Table 4.6: Fuel weight fraction for each segment of the mission.

#	Mission Segment	Fuel Weight Fraction
1	Engine start-up (Taxi) and take-off (TO)	0.970
2	Climb and acceleration to cruise	0.985
3	Cruise (Range)	$exp \cdot \left[\frac{-R \cdot SFC}{V \cdot \frac{L}{D}}\right]$
4	Loiter (Endurance)	$exp \cdot \left[\frac{-E \cdot SFC}{\frac{L}{D}}\right]$
5	Descent	1.000
6	Landing	0.995

Observing table 4.6 there are two segments of the flight that need further analysis in order to fully comprehend the strategy behind the designing of the LH_2 conceptual aircraft, which are the cruising phase and the loiter or holding phase.

The cruising phase fuel weight fraction can be given by the Breguet equation seen on the table 4.6 and, for the sake of illustration, also below:

$$\left[\frac{W_3}{W_2}\right] = exp \cdot \left[\frac{-R \cdot C_{cruise}}{V_{cruise} \cdot \left(\frac{L}{D}\right)_{cruise}}\right] \tag{4.29}$$

The variables and values used to solve this equation (4.29) are summarized on table 4.7.

Table 4.7: Breguet's equation for cruise variables values.

Property	Symbol	Unit	Value
Range	R	ft	18289107.612
Specific Fuel Consumption	$SFC_{cruise_{-LH_2}}$	$lb_{fuel}/lb_{thrust} \cdot s$	6.148×10^{-5}
Velocity	V_{cruise}	ft/s	767.352
Gliding ratio	L/D_{cruise}	-	17.260

The specific fuel consumption (SFC) was calculated by converting the SFC of kerosene fuelled engines, $SFC_{Kerosene}$, to a LH_2 fuelled engine's SFC (SFC_{LH_2}). According to the experimental relation provided by Boggia [32]. This experimental relation states that there is a 63.6% decrease in the SFC of LH_2 fuelled engines when compared to kerosene fuelled engines.

$$SFC_{LH_2} = 0.364 \cdot SFC_{Kerosene} \tag{4.30}$$

The loiter's phase fuel weight fraction is given by Breguet's equation for endurance (table 4.6). The following table contains the parameters defined for this flight segment.

Table 4.8: Breguet's equation for loiter variables values.

Property	Symbol	Unit	Value
Endurance	E	min	30
Specific Fuel Consumption	$SFC_{loiter_{-\mathrm{LH_2}}}$	$lb_{fuel}/lb_{thrust} \cdot s$	4.841×10^{-5}
Gliding ratio	L/D_{loiter}	-	19.931

Similarly to what has been shown for the cruising flight segment, the SFC for LH_2 fuelled engines can be obtained by converting the SFC of kerosene fuelled engines (for loiter phase) with the help of the relation presented before (4.30). The endurance was set to 30 minutes and the gliding ratio for loiter was obtained by the following relation [39]:

$$\left(\frac{L}{D}\right)_{loiter} = \frac{\left(\frac{L}{D}\right)_{cruise}}{0.866} \tag{4.31}$$

4.4.1.2 LH_2 MTOW calculation and fuel tank length determination

Having obtained the weight fractions of the aircraft, it is now possible to assemble all the knowledge obtained so far. This includes details about the tank geometry and it's unitary volume and dry mass and combine them in such a way that one can achieve an iterative set of equations that can provide the final characteristics of the conceptual LH_2 aircraft.

The first equation is derived from equation 4.25 and can be seen below:

$$W_{TO} = \frac{W_{payload} + W_{passengers}}{1 - \frac{W_{fuel}}{W_{TO}} - \frac{W_{\mathrm{LH_2}'A/C-empty}}{W_{TO}}} \tag{4.32}$$

The empty weight of the conceptual LH_2 aircraft will be given by the sum between the total dry mass of the hydrogen fuel tanks (taking into account the total length of the tank, which is yet to be determined) and the empty weight of the conceptual LH_2 aircraft without accounting for the tank's dry mass, $W_{\mathrm{LH_2}'A/C-empty-notanks}$, which has been calculated earlier (expression 4.27). As such, the following equation is arranged:

$$W_{\mathrm{LH_2}'A/C-empty} = W_{\mathrm{LH_2}'A/C-empty-notanks} + W_{tank} \tag{4.33}$$

The following equation allows for the introduction of another variable regarding the tank design:

$$W_{tank} = W_t \cdot l_s + W_{sphere} \tag{4.34}$$

Where W_{tank} represents the total dry mass of the LH_2 tank. W_t is the dry mass of the tank per unit length (of the cylindrical shaped part of the LH_2 tank) and naturally, l_s is the length that the tank needs in order to contain (also regarding the cylindrical shaped part of the tank) enough fuel to complete the proposed mission (section 4.2). Lastly, W_{sphere} stands for the two semi-spherical ends of the tank that

seal the LH_2 tank. According to the methodology employed in the tank design section, it's dry mass can be calculated *a priori*.

Concerning the fuel quantity the following relation can be arranged:

$$\prod_{k=1}^{k=6} \frac{W_k}{W_{k-1}} = \frac{W_{fuel}}{W_{TO}} \tag{4.35}$$

Where $\prod_{k=1}^{k=6} \frac{W_k}{W_{k-1}}$ is the product of all the fuel fractions of each segment k of the mission (please revisit table 4.6). W_{fuel} is the weight of the fuel needed to complete the mission and W_{TO} is the MTOW of the LH_2 aircraft.

The final equation required for the sizing of the conceptual LH_2 aircraft relates the weight of the fuel to the dimensions and volume of the hydrogen tank.

$$W_{fuel} = V_t \cdot l_s \cdot \rho_{LH_2} + V_{sphere} \cdot \rho_{LH_2} \tag{4.36}$$

Where V_t is the volume per unit length of the cylindrical shaped part of the tank. ρ_{LH_2} is the density of the LH_2 at the temperature and pressure that the tank is designed for. V_{sphere} is the known volume of the two semi-spherical ends of the LH_2 tanks.

MATLAB scripts have been devised in order to fully solve these equations iteratively and provide the user with the results/outputs listed in table 4.9. Figure 4.7 is a flowchart that comprises the main steps of the strategy undertaken in order to size the conceptual LH_2 fuelled aircraft. This flowchart also summarizes the most important mission requirements imposed upon this strategy and reveals the final outputs that are also represented in table 4.9 as previously stated.

Table 4.9: Conceptual LH_2 aircraft outputs.

Output description	Symbol
Maximum Take-Off Weight	W_{TO}
Fuel Weight	W_{fuel}
LH_2 Tank Dry Mass	M_{tank}
LH_2 Tank Lenght	l_t
Operating empty weight (including LH_2 tanks)	$W_{LH_2'A/C-empty}$
Total LH_2 aircraft length	$L_{LH_2'A/C}$

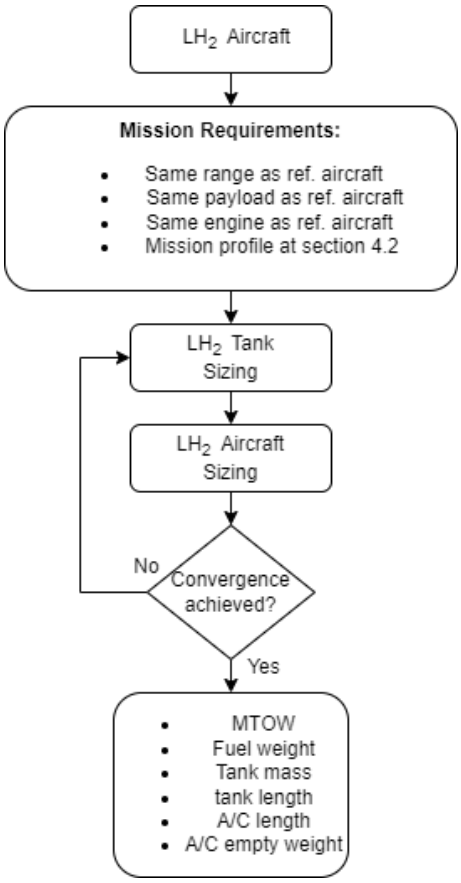

Figure 4.7: Conceptual LH_2 aircraft design strategy flowchart.

4.5 Life Cycle Assessment

In order to validate the feasibility of the implementation of an aircraft fuelled by LH_2 when compared with a kerosene fuelled aircraft in terms of environmental impacts, resource depletion and human health impact, a life cycle assessment (LCA) is to be performed.

In more recent times, the general awareness of the need to protect the environment has increased substantially. For this reason the environmental impacts of new or altered manufactured products need to be studied and predicted. The increasing demand for predicting and studying these impacts has led to the creation of some tools and methodologies, being the LCA one of them [56].

The LCA is a very powerful methodology to identify and improve certain aspects of a product's life cycle by diminishing it's environmental impact. The LCA can provide critical information to help decision-makers make better and more conscious decisions regarding the preservation of the environment, select techniques and performance indicators regarding environmental preservation and lastly, assist in marketing [56].

According to ISO 14040:2006 standard [57], the LCA is comprised of the following four phases (illustrated schematically in figure 4.8):

- Goal and scope definition

- Inventory analysis
- Impact assessment
- Interpretation

The goal and scope phase contemplates the boundary definition, detail level of the life cycle assessment and the intended use and motives for the LCA study. The inventory analysis consists in the gathering of data regarding the resources and raw materials associated with the processes that compose the phenomena in study. This collection of inflow and outflow data is what allows to reach the goal proposed in the previous step. The impact assessment's phase purpose is to better understand the inventory and to determine it's significance related to the end goal. The last phase of the life cycle assessment is the interpretation and it consists on the discussion and analysis of the previous phase's results in order to be able to take decisions or provide recommendations that ensure a lesser impact on the environment. All previous definitions are described with more detail in a British standards report [56].

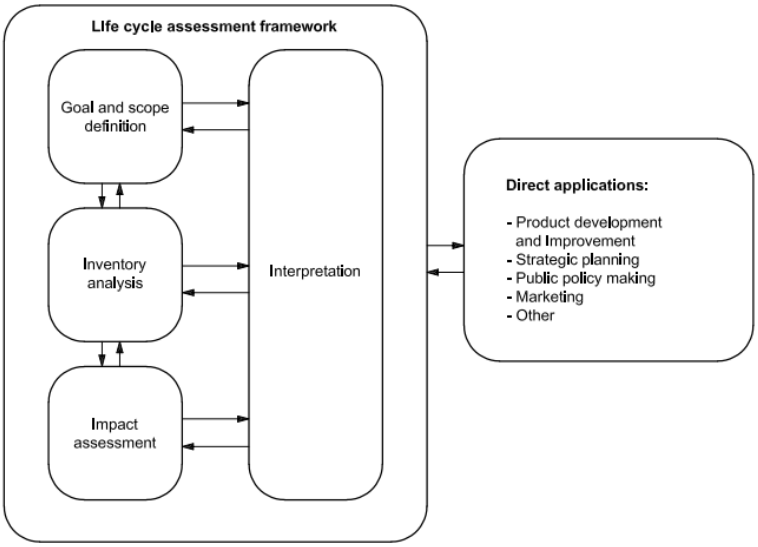

Figure 4.8: Life Cycle Assessment phases - ISO 14040:2006 [56]

4.5.1 Goal and scope definition

The clear goal of this LCA is the characterization and evaluation of the environmental impacts that would be consequence of the implementation of LH_2 fuelled aircraft of medium range. Such study implies the comparison between different hydrogen production methods and techniques, along with the contribution from the combustion of this fuel in it's liquid form as consequence of the aircraft's operation.

Another crucial part of this LCA is to include the production of kerosene fuel and it's combustion during flight for the selected reference aircraft and determine it's environmental impacts. This analysis is essential to compare the environmental competitivity between a traditional kerosene fuelled aircraft and a yet conceptual LH_2 fuelled aircraft.

Regarding hydrogen production methods, four methods were selected:

- SMR
- Coal gasification with CCS technology
- Wind powered electrolysis
- Solar powered photo-voltaic (PV) electrolysis

These methods were selected to provide a solid basis that enriches the comparison between grey hydrogen, blue hydrogen and green hydrogen. SMR was selected as the grey hydrogen representative method since this production method accounts for 45% of hydrogen production and it is the most common hydrogen production method, as explained in section 2.4.

Coal gasification with CCS technology was selected as the blue hydrogen production method due to it's promising results in this hydrogen LCA study [58].

Wind and PV electrolysis were selected as the green production methods given their promising results on this study [59]. More information regarding the production and inventory for these four methods will be provided further in this section.

Functional Unit

Regarding the functional unit, most studies related to hydrogen LCA's use as a functional unit the Tonne-Kilometre (tkm) which represents the transport of one tonne of goods (payload) by any mean of transportation (in this case, an aircraft) for one kilometre travelled. As stated by Dincer et al. [59], this method, unlike the use of Passenger-Km, accounts for all the emissions of the flight and production phases. For the previous reason this unit will also be adopted in this thesis for the sake of result comparison and discussion with the existing literature about this subject.

System Boundary

As it has been previously stated, only the production of the fuel and, posteriorly, it's combustion during the aircraft's operation are to be studied in this LCA, as such, inventory for the resources needed for the production of the fuel and the emissions generated by this process along with the emissions generated by the burning of fuel during flight has been collected and taken into consideration. In other words, the emissions from the aircraft's operation represent the final boundary of this LCA and are absolutely crucial to fully assess the impacts of hydrogen fuelled aircraft.

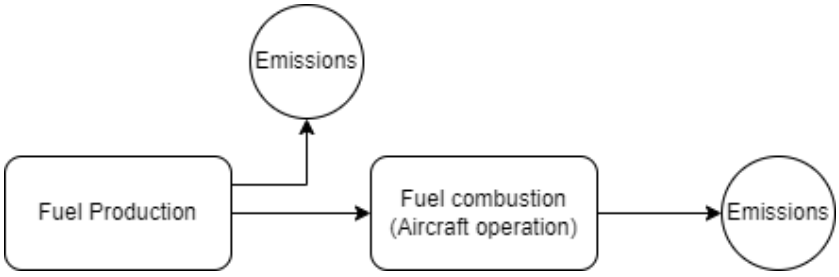

Figure 4.9: Boundaries of the LCA.

Impact categories

The impact categories chosen for this study are enumerated below in table 4.10. The units are also displayed and are retrieved from SimaPro manual [60]:

Table 4.10: LCA impact categories.

Impact categories	Unit
Climate change	Kg CO_2 eq.
Terrestrial acidification	Kg SO_2 eq.
Marine eutrophication	Kg N eq.
Human toxicity	Kg 1.4-DB eq.
Photochemical oxidant formation	Kg NMVOC eq.
Particulate matter formation	Kg PM-10
Fossil depletion	Kg Oil eq.

LCA limitations

The transportation of fuels from the refinery to the operating airport has been discarded since it varies greatly depending on what continent, country or even city in which the airport is operating on, and would only be a good addition in a less generalist approach. Due to small differences regarding the structure of both aircraft's (conceptual LH_2 aircraft and reference aircraft) a study considering the building of each aircraft and it's disposal has also been discarded since it would not make much difference in the end results.

4.5.2 Life Cycle Inventory (LCI)

The life cycle inventory phase will be divided into three parts, one part regarding the inventory for kerosene production. The second part presents the inventory for LH_2 production methods. The third and last part reveals an inventory for the combustion of both fuels. These inventories were collected through a literature research and complemented by Ecoinvent libraries. The results for each impact category were computed with the aid of SimaPro computer software.

4.5.2.1 Hydrogen production LCI

Steam methane reforming

According to the United States of America Department of Energy [25], SMR is a well implemented and tried hydrogen production method. It makes use of existing natural gas pipeline infrastructure and represents nearly 95% of all hydrogen produced in the United States.

In SMR process, methane reacts with a very high temperature steam at pressures between 3 and 25 bar in a catalyst. These reactions result in the formation of hydrogen, carbon monoxide and very

small quantities of carbon dioxide. Then, the CO resulting from the first reaction is mixed with more high temperature steam and, using a catalyst, produces CO_2 and more hydrogen. This second procedure is known as water-gas shift reaction. Finally, CO_2 is removed, leaving only hydrogen [25]. Below the chemical reaction formulas inherent to SMR are displayed.

$$CH_4 + H_2O \longleftrightarrow CO + 3\,H_2 \tag{4.37}$$

$$CO + H_2O \longleftrightarrow CO_2 + H_2 \tag{4.38}$$

The inventory to simulate the impact hydrogen production by SMR has on the environment was retrieved from a LCA performed by Cetinkaya et al. [61] and then SimaPro software was used to calculate the impact categories that will be analyzed in the following chapter.

Coal gasification with CCS technology

The second and last hydrogen production method analyzed on this thesis that involves the direct use of fossil fuels is the coal gasification with CCS technology. According to the United States of America Department of Energy [25], the first stage of this production method consists in reacting steam, coal and oxygen at high temperatures and pressures. As a result of this procedure a gas composed essentially of hydrogen and CO (equation 4.39) is created. After the removal of the impurities, more hydrogen is produced by reacting the previous gas mixture with high temperature steam in what is called a water-gas shift (equation 4.38). As seen previously for the SMR production method, the water-gas-shift reaction also produces CO_2 which is separated from the hydrogen and posteriorly captured and stored.

Regarding the inventory of this production pathway, ecoinvent library was used along with SimaPro software in order to obtain the resulting values for the impact categories mentioned earlier.

Coal gasification reaction:

$$CH_{0,8} + O_2 + H_2O \longleftrightarrow CO + CO_2 + H_2 + \text{Impurities} \tag{4.39}$$

Wind and Photo-voltaic electrolysis

Electrolysis consists in splitting water molecules into it's two components, hydrogen and oxygen, a feat that is accomplished through the use of electricity. This reaction takes place in an electrolyzer unit. An electrolyzer is a system composed of a cathode and an anode which are separated by an electrolyte. The electrolyzer system can vary somewhat due to the type of electrolyte that is used [25]. For the sake of simplicity, only polymer electrolyte membrane (PEM) electrolyzers will be considered in this analysis.

In a PEM electrolyzer, water reacts at the anode, splitting it into oxygen and positively charged hydrogen ions. The resulting electrons are thrown into a secondary circuit and the hydrogen ions are then selectively moved across the electrolyte membrane in order to react at the cathode with the electrons, thus creating neutral hydrogen atoms [62].

Anode reaction:

$$2\,H_2O \longleftrightarrow O_2 + 4\,H^+ + 4\,e^- \tag{4.40}$$

Cathode reaction:

$$4\,H^+ + 4\,e^- \longleftrightarrow 2\,H_2 \tag{4.41}$$

The electricity involved in this process can have different origins, however only electricity produced from wind energy and solar energy (harnessed by photo-voltaic panels) are to be considered since they are prone to produce a much lesser impact on the environment. Also, since other energy sources (fossil fuels) have been already considered in this work, having these energy sources also studied is of the uttermost importance in order to ensure a more diverse study and thus, a more complete LCA.

Similarly to SMR production method, the inventory for wind powered electrolysis was retrieved from [61] and the impact categories were obtain with SimaPro software. Solar energy powered electrolysis was simulated using ecoinvent library and SimaPro software. Table 4.11 displays the inventory gathered for SMR and wind electrolysis [61].

Table 4.11: Inventory for SMR and wind electrolysis regarding the production of one kilogram of H_2, based on Cetinkaya et al. [61].

	SMR [g/Kg H_2]	Wind Electrolysis [g/Kg H_2]
Economic inflows		
Coal (in ground)	–	157.4
Iron (Fe, ore)	–	148.5
Iron scrap	–	105.2
Limestone ($CaCO_3$ in ground)	–	355.5
Natural gas (in ground)	3528.78	14.2
Oil (in ground)	–	43.1
Water (H_2O)	18800	22161
Average air emissions		
CO_2	8756.1	783.75
CO	0.07	0.75
CH_4	–	0.29
NO_x	0.82	4.37
NO	–	0.03
Non CH_4 hydrocarbons	–	3.07
Particulates	0.02	27.24
SO_x	–	5.36
Benzene	0.27	–

4.5.2.2 Kerosene production LCI

Kerosene production inventories are available at ecoinvent library, which was used alongside SimaPro software in order to obtain the resulting values for the impact categories mentioned earlier. As such, it is now possible to compare all the selected hydrogen production methods and the production of traditional kerosene.

4.5.2.3 Hydrogen and kerosene combustion LCI

As mentioned earlier on this thesis, the burning of each fuel can emit considerable quantities of GHG and other undesirable gases to the atmosphere, as such, it is necessary to gather relevant inventory regarding the emissions of both kerosene and hydrogen combustion at high temperatures. Table 4.12 summarizes the emissions that result from the combustion of each fuel:

Table 4.12: Combustion reagents and products of LH_2 and kerosene fuels, values were retrieved from [13].

	Kerosene [g/Kg Kerosene]	LH_2 [g/Kg H_2]
Combustion reagent		
O_2	3400	8000
Combustion products		
CO_2	3150	–
CO	3,7	–
H_2O	1250	9000
NO_x	14	4,3
SO_x	1	–
Soot	0,04	–
UHC	1,3	–

With the inputs of the table above, it is possible to calculate the values for the impact categories with the aid of SimaPro computer software.

Chapter 5

Results & discussion

In order to truly assess the environmental and economic impacts of transitioning from kerosene fuelled aircraft to LH_2 fuelled aircraft, this chapter contemplates the results given by the methodology introduced in the previous chapter. This way it is possible to compare the main aircraft specifications between both types of fuels. This chapter is comprised of three main segments, primarily the presentation of the results obtained for the sizing of the conceptual LH_2 aircraft with the MATLAB script and comparison with the reference aircraft, secondly a discussion related to the results obtained with the LCA and finally, an economic assessment is performed regarding the economic competitiveness of each fuel and their production methods.

5.1 Conceptual LH_2 aircraft simulation

Table 5.1: Detailed overview and comparison between the conceptual LH_2 aircraft and the reference aircraft.

	Unit	Conceptual LH_2 aircraft	Reference aircraft	Difference (%)
A/C properties				
MTOW	Kg	76354	79016	−03.37
Empty weight	Kg	44747	41413	08.05
LH_2 tank dry mass	Kg	2466	–	–
Fuel weight	Kg	10006	16284	−38.46
Energy Consump.	GJ	1202.4	732.8	64.09
Aircraft length	m	46.67	38.08	22.56
Aircraft diameter	m	3.76	3.76	00.00
Emissions				
CO_2	Kg	–	51295	−100.00
NO_x	Kg	43	228	−81.10
H_2O	Kg	90184	20355	343.05
CO	Kg	–	60	−100.00
SO_x	Kg	–	16	−100.00
Soot	Kg	–	0.65	−100.00
UHC	Kg	–	21	−100.00

According to the previous table, it is possible to infer that the LH_2 conceptual aircraft has a lower MTOW than the reference kerosene fuelled aircraft (-3.37%) despite possessing a higher empty weight. This is due to the lower fuel weight displayed by the LH_2 aircraft (-38.46%), which, in turn, is a direct consequence of the higher specific energy inherent to LH_2 fuel.

The empty weight of the conceptual LH_2 aircraft is 8.05% higher than the reference aircraft, this is explained mostly due to the extra weight added by the cryogenic tanks and the extra length of the LH_2 aircraft imposed by the fitting of these same tanks.

In sum, although the operation of a LH_2 fuelled aircraft inherently means a 64.09% higher energy consumption and an increase of about 8.6 meters of the aircraft's fuselage, there is an unquestionable reduction in hazardous emissions to the atmosphere. As expected, there are no CO_2 emissions, which is one of the most significant global warming gasses and also, using LH_2 as an aviation fuel would mean no CO, SO_x, soot or UHC emissions to the atmosphere. The combustion of LH_2 also means a reduction of about 81.10% in NO_x emissions when compared to the combustion of kerosene. The only chemical component that the operation of a LH_2 fuelled aircraft emits in higher quantities than the reference aircraft is H_2O, which is almost four and a half times greater for the LH_2 aircraft.

However, in order to truly assess the environmental superiority of a LH_2 fuelled aircraft, it is essential to evaluate hydrogen production methods and it's environmental impacts, such analysis will be carried out in the next sections along with an economic feasibility study for this fuel.

The following figure (figure 5.1) is the result of a sensitivity analysis regarding the evolution of the MTOW of the LH_2 conceptual aircraft with a reduction in the lift-to-drag ratio ($\frac{L}{D}$). This analysis was

carried out since the theoretical model implemented in the previous chapter does not account for the increase of frictional drag due to the increased length of the fuselage. This increase in drag would lead to a reduction of the lift-to-drag ratio and, consequently, an increase of the MTOW.

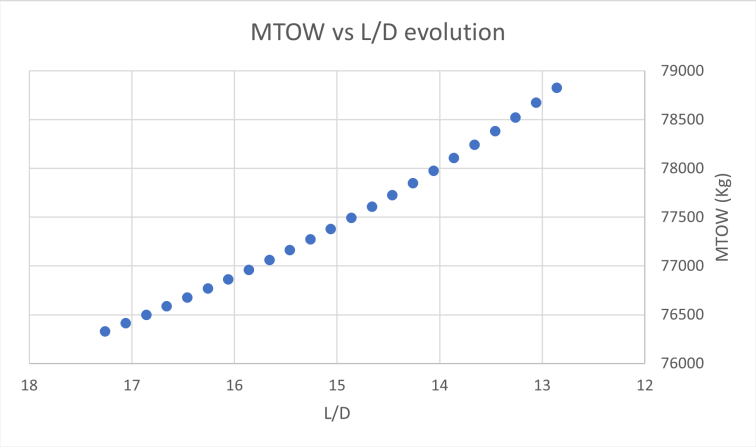

Figure 5.1: MTOW vs $\frac{L}{D}$ evolution.

5.2 Environmental impacts

In order to further compare the differences inherent to the usage of each fuel and it's production method, a LCA was carried out. The aircraft's specifications obtained at the previous section were used as a basis for this LCA. The following graphs (figure 5.2) represent the results obtained from SimaPro computer software for each of the categories set to be studied at section 4.5.1. The graph of each impact category already exhibits the combination (sum) of the results obtained for the production step of the LCA (fuel production method) and the results obtained due to the emissions originated from the fuel combustion during flight (design mission 4.2). To ensure the best comparison possible, the results are presented in kilograms per tonne-kilometer for every impact category.

Regarding the climate change (figure 5.2 a)) indicator or, in other words, global warming potential indicator (GWP), traditional kerosene fuel possesses the highest GWP, a value of 0.8348 Kg CO_2 eq./tonne-km closely followed by LH_2 produced by SMR which has a GWP only 1.1% lower than traditional kerosene. Although the combustion of LH_2 produces very few GHG emissions to the atmosphere, the overall GWP is almost the same between LH_2 produced by SMR and traditional kerosene. This fact truly reinforces the premise that the production method from which LH_2 is produced is essential for this comparison since there would be very little gain in transitioning from kerosene fuelled aircraft to LH_2 fuelled aircraft if the LH_2 is produced by SMR. Wind energy electrolysis is the production method with the least GWP, having an impact 90.9% lower than traditional kerosene and it also has a GWP of 68.5% lower than coal gasification with CCS which is the least impactful fossil fuel based production method with a value of 0.0758 Kg CO_2 eq./tonne-km. PV electrolysis despite being very competitive regarding low GHG emissions still has 29.4% higher GWP than wind energy electrolysis.

Observing figure 5.2 b), traditional kerosene fuel is presented as the highest contributor to terrestrial

acidification due to the deposit of acidifying substances in terrestrial ecosystems. Although LH_2 produced from renewable energy sources (wind and PV) have much less impact in terrestrial acidification than traditional kerosene (less 70.8% and 74.0% impact for wind energy and PV energy electrolysis, respectively), SMR and coal gasification with CCS both present better results for this indicator despite having fossil fuels as their primary energy source.

For marine eutrophication traditional kerosene also presents the highest impact results followed by PV energy electrolysis and wind energy electrolysis. Similarly to what was seen for terrestrial acidification, LH_2 produced by SMR and coal gasification with CCS also present less impactful results than LH_2 produced from renewable energy sources.

Traditional kerosene possesses the highest toxicity (figure 5.2 d)) of all production methods being studied, more than 87% of the toxic emissions is due to kerosene combustion, far greater than the emissions resulting from it's production. PV energy electrolysis also possesses high toxicity levels, however, 52.1% lower than traditional kerosene. Wind energy electrolysis and SMR LH_2 have almost no toxicity levels. PV energy electrolysis toxicity result may be explained due to solid-wastes and flammable-substances resulting of the production stages [63].

Attending on figure 5.2 e), the production method with the highest particulate formation per tonne-km is traditional kerosene. SMR produces the least particles, about 90.1% less than traditional kerosene kerosene. All LH_2 production methods are somewhat even on this indicator with the fossil fuel primary energy methods outperforming the renewable methods of LH_2 production.

Due to high NO_x emissions (both in the production stages as well as during the flight stage), traditional kerosene is considerably more impactful than any LH_2 production method in regard to the particulate oxidant formation metric (figure 5.2 f)). the second highest is PV energy electrolysis however, it represents a value 85.1% lower than traditional kerosene. The least harmful LH_2 production method is SMR.

Unsurprisingly, the production methods which use fossil fuels as their primary energy source are clearly leading the fossil depletion metric (figure 5.2 g)). Traditional kerosene is, as in all other impact categories, the production method that has the highest environmental impact in fossil depletion, followed by SMR and coal gasification with CCS. LH_2 renewable production methods have very little impact in terms of fossil depletion.

This LCA allows one to conclude that LH_2, regardless of the production method is consistently less environmentally harmful than kerosene. LH_2 produced by SMR although it proved to be the least harmful production method in five of the seven impact categories studied on this thesis it has quite an impact in global warming potential (virtually the same as traditional kerosene). Also regarding LH_2 production methods with fossil fuels as primary energy source, coal gasification with CCS proved to be a good alternative for hydrogen production. The renewable LH_2 production paths chosen proved to be much less harmful than kerosene in all impact categories, with a clear advantage for wind energy electrolysis in terms of GWP. PV energy electrolysis scored very high for human toxicity.

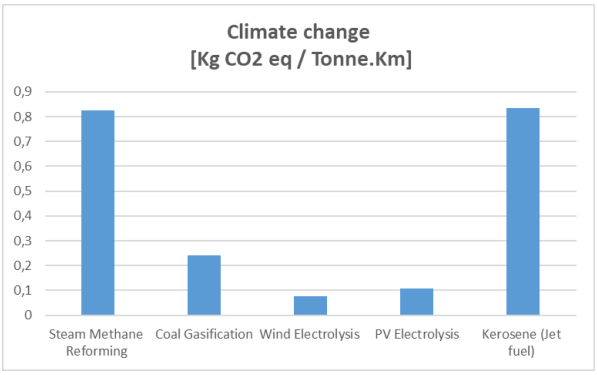

(a) Climate change indicator (GWP)

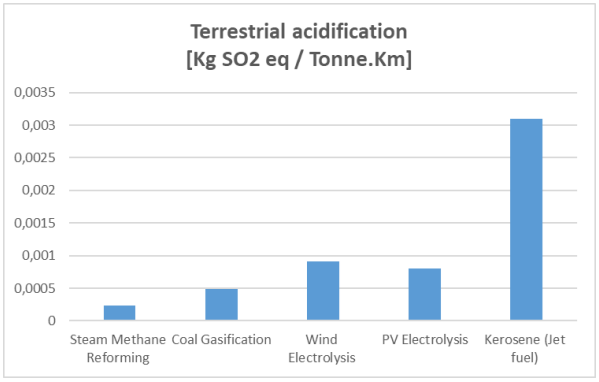

(b) Terrestrial acidification indicator

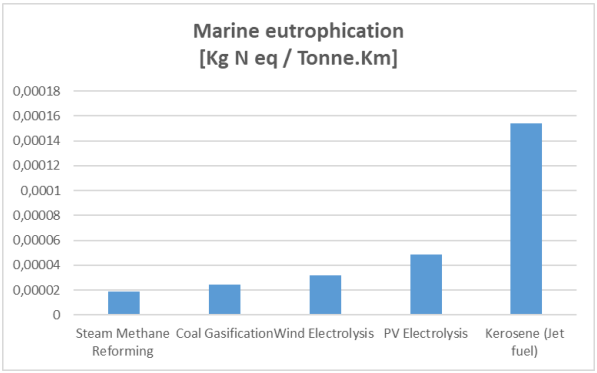

(c) Marine eutrophication indicator

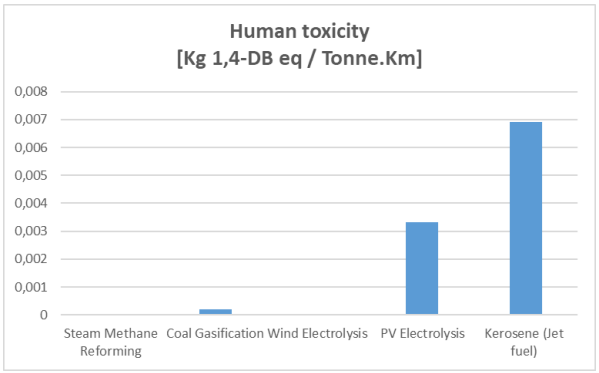

(d) Human toxicity indicator

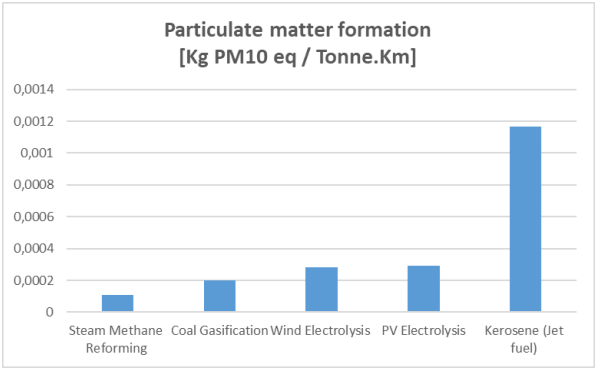

(e) Particulate matter formation indicator

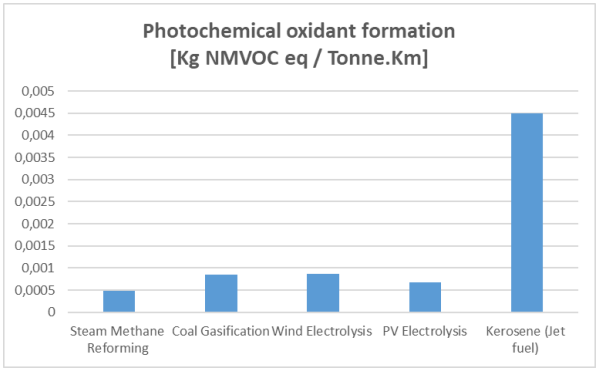

(f) Particulate oxidant formation indicator

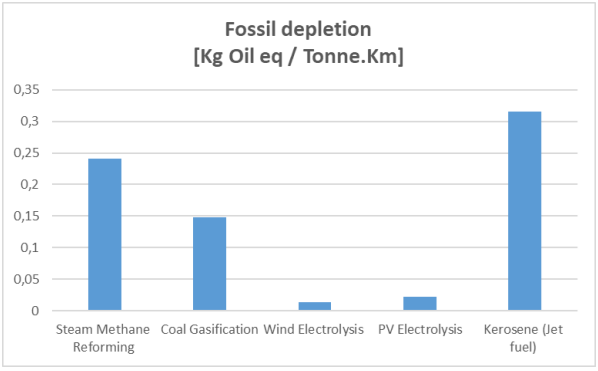

(g) Fossil depletion indicator

Figure 5.2: Impacts generated by different production methods and different fuel combustion.

5.3 Fuel production and selling price

The LCA previously executed made it possible to assess the environmental impact of both fuels and their production methods, however, in order to further explore this topic it is necessary to assess the economic competitiveness of LH_2 as an aviation fuel.

The wholesale price of LH_2 is assumed to be comprised of three main factors, it's production cost, the cost inherent to it's compression, storage, and dispensing (CSD) and finally, the refining margin of the refinery.

Similarly to the approach taken for the LCA section and in order to complement it, the same four methods of LH_2 production were selected as well as the production of traditional kerosene to provide a comparing reference.

The production costs are assumed to be comprised by the cost of feedstock, the cost of operation and maintenance (O&M) and capital costs. Capital costs can be attributed to infrastructure and equipment. The following table summarizes the production and CSD costs for the chosen production methods [64].

Table 5.2: Production and CSD costs for different LH_2 production methods [64] [65].

Production method	Production cost ($ /Kg_{LH_2})	CSD cost ($ /Kg_{LH_2})
SMR	1.97	3.38
Coal gasification with CCS	2.06	3.38
Electrolysis - Wind	4.27	3.38
Electrolysis - PV	5.78	3.38

The following chart (figure 5.3) represents the wholesale price for LH_2 fuel and shows the contribution of each of the three factors mentioned earlier. For the sake of comparison traditionally produced kerosene fuel is also plotted.

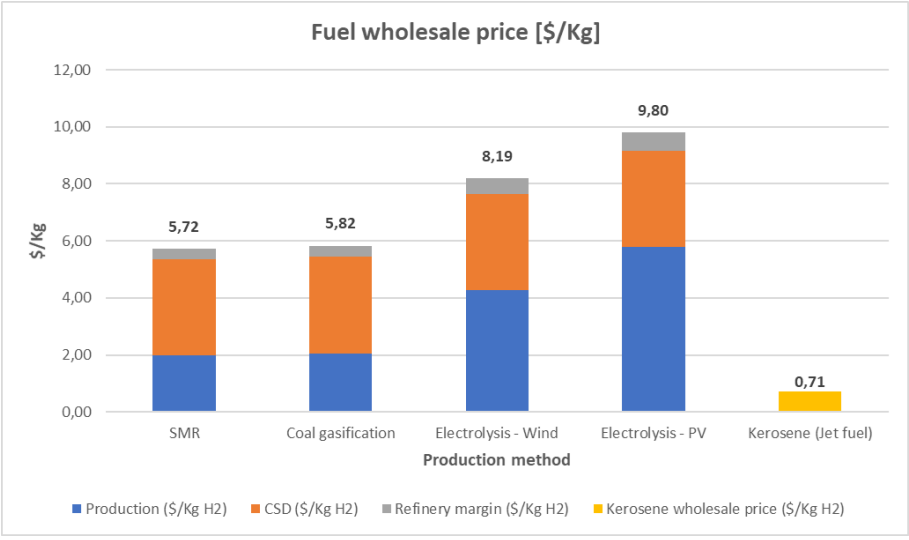

Figure 5.3: Fuel wholesale price aggregate.

The refining margin was assumed to be 7%, this methodology was also undertaken by the United States Department of energy [66]. Beware, however, that the real refining margin could be very volatile as can be seen in oil industries, where this margin can vary greatly in short periods of time due to a wide variety of economical factors. The wholesale price of kerosene was retrieved from IATA's Jet Fuel Price Monitor [67] after the effects of SARS-COV-2 on jet fuel price had subsided and back to pre pandemic levels in order to provide a more fair comparison between each fuel.

The cost of liquefaction of hydrogen gas is already contemplated on the CSD costs which are equal for every production method listed in this thesis.

Observing figure 5.3, it is clear that the wholesale pricing per kilogram of hydrogen is much higher than the wholesale price per kilogram for traditionally produced kerosene fuel regardless of the production method. Another conclusion that can be taken is that hydrogen produced from renewable energy sources through electrolysis is somewhat more expensive than those produced with fossil fuels as their primary energy source, however, according to Hydrogen Council [68], the cost of renewable hydrogen produced from wind energy in Europe is expected to decrease 60% by 2030 due to increased scale in electrolyser manufacturing, larger infrastructures and lower cost renewable energy. If this scenario holds true, then liquefied hydrogen produced by wind power electrolysis would have a production cost of 1.71 $/Kg and a wholesale price of 5.44 $/Kg of liquefied hydrogen assuming that CSD costs would remain unaltered during this time span. Thus, wind powered electrolysis would be economically more competitive than current day fossil fuel based production methods.

Regarding the high production costs of renewable energy based hydrogen production methods, feedstock costs seem to be the largest contributor to this equation, representing roughly 78% of the total production cost for wind powered electrolysis and PV powered electrolysis. In order to make these production methods more competitive, these feedstock costs need to be lowered and it is expected to happen according to the 2030 projections mentioned earlier.

The Carbon Offsetting and Reduction Scheme for International Aviation (CORSIA) could also have a positive impact in further reducing the production cost of hydrogen produced by renewable sources since the purchase of offset credits that enable airlines to compensate for emissions exceeding the baseline set at the year of 2020 contribute to reducing emissions in several sectors of the economy such as renewable energies [69].

CSD costs have quite an impact in the wholesale price of hydrogen regardless of production method, representing about 30.5% of the total wholesale price of hydrogen produced by SMR and 21.3% of the wholesale price of wind powered electrolysis (both of which have the lowest wholesale price of the fossil based primary energy source and renewable primary energy source, respectively). As such, a reduction on CSD costs could have a major role in turning liquefied hydrogen economically more competitive in comparison with kerosene fuel and thus promoting lesser environmental impacts. The National Renewable Energy Laboratory [64], also points out the necessity of supporting R&D (Research and Development) towards the diminishing of CSD costs.

Connecting the results obtained in the previous section (section 5.2) to the economic competitiveness assessment, one can conclude that liquefied hydrogen produced by coal gasification with CCS

technology is much less environmentally damaging than traditional kerosene. Particularizing on the GWP indicator, coal gasification with CCS it is quite superior to traditional kerosene and not much inferior to renewable energy powered electrolysis. Coal gasification with CCS technology besides proving to be an environmentally competitive hydrogen production method, at the current date it is also economically more competitive than wind powered electrolysis (which is the most competitive renewable hydrogen production method both in terms of LCA indicators and economic competitiveness).

In section 5.1, it was noted that the conceptual LH_2 aircraft needed considerably less fuel weight than the reference kerosene aircraft to perform the design mission, as such, it is of added value to assess the fuel cost difference for each of the hydrogen production methods evaluated in this thesis. The following table (5.3) displays the resulting values in order to perform this fuel comparison:

Table 5.3: Fuel cost per tonne-kilometer of different fuels and production methods.

	Unit	Conceptual LH_2 aircraft	Reference aircraft	Difference (%)
SMR	\$/Tonne-km	0.4767	–	395.74
Coal gasification	\$/Tonne-km	0.4847	–	404.09
Electrolysis - Wind	\$/Tonne-km	0.6816	–	608.87
Electrolysis - PV	\$/Tonne-km	0.8161	–	748.79
Traditional kerosene	\$/Tonne-km	–	0.0962	0.00

Although the fuel weight is considerably less for the LH_2 conceptual aircraft than the reference kerosene aircraft (-38.46%), the highly expensive liquefied hydrogen imposes, even for the best case scenarios, a fuel expense about five times greater than the fuel expense shown for the reference aircraft. However, despite the high wholesale prices of liquefied hydrogen, this fuel produces far less environmentally damaging emissions if produced by one of the following methods, coal gasification with CCS technology, wind energy electrolysis and PV (solar) energy electrolysis.

Chapter 6

Conclusions

The usage of LH_2 as an aviation fuel instead of kerosene is unquestionably a much better option for the preservation of the environment during aircraft operation, since it's combustion produces less quantities of GHG and other environmentally harmful gases. However, the production method used to produce hydrogen can greatly influence whether or not hydrogen fuelled aircraft can be environmentally better than traditional aircraft. The LCA carried out in this thesis concluded that wind energy source electrolysis (green hydrogen), especially in terms of GWP, is environmentally better than traditional kerosene, and also, it is the best hydrogen production method to reduce GHG emissions to the atmosphere, and thus, the best option to achieve the target of limiting global warming to 1.5 degrees Celsius relatively to pre-industrial levels.

Despite the very promising results exhibited by renewable energy source electrolysis in the LCA, these hydrogen production methods lead to a high wholesale price and thus, it becomes less competitive when compared to hydrogen produced by SMR and coal gasification with CCS technology, which are the production methods representing grey and blue hydrogen, respectively. Also, regardless of the production method, hydrogen is considerably less economically competitive than traditional kerosene. However, if projections hold true, in 2030, wind energy electrolysis will become much more competitive than any hydrogen production method available today and only 370% more expensive than traditional kerosene when adjusted for the proposed design mission, assuming that CSD costs remain unchanged during this time span.

Coal gasification with CCS technology proved to be very consistent in both the LCA and the economic assessment performed in this thesis, obtaining good results for many impact indicators as well as being one of the most economically competitive hydrogen production methods (possessing a wholesale value 30% lower than wind energy powered electrolysis). Given these facts, while wind energy remains expensive, coal gasification with CSS technology presents itself as a solid mid term option for hydrogen production.

Regarding the LH_2 aircraft itself, in order to accommodate the cryogenic tanks a considerable increase in length is to be expected, however, the MTOW is slightly lower than the reference kerosene fuelled aircraft. A higher energy consumption is also to be expected when transitioning from traditional

aircraft to LH_2 fuelled aircraft but due to the higher specific energy displayed by the LH_2, the fuel weight of the LH_2 fuelled aircraft is in fact lower than the fuel weight exhibited by the reference kerosene aircraft.

6.1 Future Work

As part of future work, it would be an added value to explore hydrogen based synfuel since it has more competitive prices than LH_2 and yet, according to the literature, these type of aviation fuels show promising results regarding the reduction of GHG and other harmful gases emitted to the atmosphere when compared to traditional kerosene.

Another technology that would be interesting to explore would be the use of hydrogen fuel cells within an aircraft. Fuel cells could prove very competitive against LH_2 since there would be no NO_x emissions to the atmosphere given the lower combustion temperatures and also, in case hydrogen is to be stored within the aircraft in it's gaseous state there could also be some differences regarding the CSD costs, and consequently, there could be some changes on it's wholesale price.

In conclusion, an economic assessment and LCA comparing hydrogen based synfuel fuelled aircraft, fuel cell powered aircraft and LH_2 aircraft should be perform in order to better understand which direction the aviation should be heading in it's quest to diminish it's impact on the environment.

Bibliography

[1] D. Lee, D. Fahey, A. Skowron, M. Allen, U. Burkhardt, Q. Chen, S. Doherty, S. Freeman, P. Forster, J. Fuglestvedt, A. Gettelman, R. D. Léon, L. Lim, M. T. Lund, R. Millar, B. Owen, J. Penner, G. Pitari, M. Prather, R. Sausen, and L. Wilcox. The contribution of global aviation to anthropogenic climate forcing for 2000 to 2018. *Atmospheric Environment*, 244, 2021. doi.org/10.1016/j.atmosenv.2020.117834.

[2] ATAG. Facts & figures (accessed: 13.12.2021). URL `https://www.atag.org/facts-figures.html`.

[3] B. Khandelwal, A. Karakurt, P. R. Sekaran, V. Sethi, and R. Singh. Hydrogen powered aircraft : The future of air transport. *Progress in Aerospace Sciences*, 60:45–59, 2013. doi: 10.1016/j.paerosci.2012.12.002.

[4] S. Gossling and A. Humpe. The global scale, distribution and growth of aviation: Implications for climate change. *Global Environmental Change*, 65, 2020. 10.1016/j.gloenvcha.2020.102194.

[5] Y. Bicer and I. Dincer. Life cycle evaluation of hydrogen and other potential fuels for aircrafts. *International Journal of Hydrogen Energy*, 42:10722–10738, 2017. 10.1016/j.ijhydene.2016.12.119.

[6] W. Group. Global warming of 1.5℃. Technical report, Intergovernmental Panel on Climate Change (IPCC), October 2018.

[7] D. Verstraete. *The Potential of Liquid Hydrogen for long range aircraft propulsion*. PhD thesis, CRANFIELD UNIVERSITY, 2009.

[8] W. Group. Airbus global market forecast 2021 - 2040. Technical report, Airbus, 2021.

[9] C. Winnefeld, T. Kadyk, B. Bensmann, U. Krewer, and R. Hanke-Rauschenbach. Modelling and designing cryogenic hydrogen tanks for future aircraft applications. *Energies*, 11(1), 2018. doi: 10.3390/en11010105.

[10] K. Seeckt and D. Scholz. Jet versus prop, hydrogen versus kerosene for a regional freighter aircraft. In *Deutscher Luft-und Raumfahrtkongress*, volume 121195. Citeseer, 2009.

[11] A. Contreras, S. Yiğit, K. Özay, and T. Veziroğlu. Hydrogen as aviation fuel: A comparison with hydrocarbon fuels. *International Journal of Hydrogen Energy*, 22, 1997. doi:10.1016/s0360-3199(97)00008-6.

[12] Fact sheet 7: Liquid hydrogen as a potential lowcarbon fuel for aviation. Technical report, IATA, August 2019.

[13] K. SEECKT. Conceptual design and investigation of hydrogen-fueled regional freighter aircraft. Master's thesis, KTH Engineering Sciences, 2010.

[14] J. S. Schutte, A. P. Payan, S. I. Briceno, and D. N. Mavris. Hydrogen-powered aircraft. *Aerospace Systems Design Laboratory*, Jan. 2010. doi:10.1002/9780470686652.eae1024.

[15] Zeppelin (accessed: 05.10.2021). URL `https://wikihmong.com/en/Zeppelins`.

[16] Meher-Homji, C. B., and E. Prisell. Pioneering turbojet developments of dr. hans von ohain—from the hes 1 to the hes 011. *Journal of Engineering for Gas Turbines and Power*, 122, 2000. 10.1115/1.483194.

[17] C.-J. Winter. Hydrogen in high-speed air transportation. *International Journal of Hydrogen Energy*, 15, 1990. 10.1016/0360-3199(80)90006-3.

[18] H. G. Klug and R. Faass. Cryoplane: hydrogen fuelled aircraft — status and challenges. *Air Space Europe*, 3, 2001. 10.1016/S1290-0958(01)90110-8.

[19] Zeppelin (accessed: 09.07.2022). URL `https://en.wikipedia.org/wiki/Zeppelin`.

[20] J.E.Penner, D.H.Lister, D.J.Griggs, D.J.Dokken, and M.McFarland. Aviation and the global atmosphere. Technical report, IPCC, 1999.

[21] Climate change 2014 synthesis report. Technical report, IPCC, 2014.

[22] M. Yu, K. Wang, and H. Vredenburg. Insights into low-carbon hydrogen production methods: Green, blue and aqua hydrogen. *International Journal of Hydrogen Energy*, 46:21261–21273, 2021. doi.org/10.1016/j.ijhydene.2021.04.016.

[23] I. Dincer and C. Acar. Review and evaluation of hydrogen production methods for better sustainability. *International Journal of Hydrogen Energy*, 40:11094–11111, 2015. doi.org/10.1016/j.ijhydene.2014.12.035.

[24] M. Ji and J. Wang. Review and comparison of various hydrogen production methods based on costs and life cycle impact assessment indicators. *International Journal of Hydrogen Energy*, 46: 38612–38635, 2021.

[25] Hydrogen production processes (accessed: 17.11.2021). URL `https://www.energy.gov/eere/fuelcells/hydrogen-production-processes`.

[26] Liquid hydrogen fuelled aircraft – system analysis. Technical report, Airbus Deutschland GmbH, 2004.

[27] Airbus - zeroe (accessed: 03.12.2021). URL `https://www.airbus.com/en/innovation/zero-emission/hydrogen/zeroe`.

[28] D. Verstraete, P. Hendrick, P. Pilidis, and K. Ramsden. Hydrogen fuel tanks for subsonic transport aircraft. *International Journal of Hydrogen Energy*, 35:11085–11098, 2010. doi:10.1016/j.ijhydene.2010.06.060.

[29] G. D. Brewer. *Hydrogen aircraft technology*. CRC Press, 1^{th} edition, 1991. ISBN 0-8493-5838-8.

[30] *The LNG task force meeting in Brussels*, November 2011. Westport Power Inc.

[31] S. K. Mital, J. Z. Gyekenyesi, S. M. Arnold, R. M. Sullivan, J. M. Manderscheid, and P. L. Murthy. Review of current state of the art and key design issues with potential solutions for liquid hydrogen cryogenic storage tank structures for aircraft applications. Technical report, NASA, October 2006.

[32] *Some Unconventional Aero Gas Turbines Using Hydrogen Fuel*, volume Volume 2: Turbo Expo 2002, Parts A and B of *Turbo Expo: Power for Land, Sea, and Air*, 06 2002. doi: 10.1115/GT2002-30412.

[33] H. Nojoumi, I. Dincer, and G. Naterer. Greenhouse gas emissions assessment of hydrogen and kerosene-fueled aircraft propulsion. *International Journal of Hydrogen Energy*, 34(3):1363–1369, 2009. doi: 10.1016/j.ijhydene.2008.11.017.

[34] C. H. Marchi and L. K. Araki. Evaluation of chemical equilibrium and non-equilibrium properties for lox/lh2 reaction schemes. *Journal of Aerospace Technology and Management*, 7(1):31–42, Jan. 2015. doi: 10.5028/jatm.v7i1.426.

[35] S. Farokhi. *Aircraft Propulsion*. Wiley, 2^{nd} edition, 2014.

[36] J. S. Kinsey, M. T. Timko, S. C. Herndon, E. C. Wood, Z. Yu, R. C. Miake-Lye, P. Lobo, P. Whitefield, D. Hagen, C. Wey, B. E. Anderson, A. J. Beyersdorf, C. H. Hudgins, K. L. Thornhill, E. Winstead, R. Howard, D. I.Bulzan, K. B. Tacina, and W. B. Knighton. Determination of the emissions from an aircraft auxiliary power unit (apu) during the alternative aviation fuel experiment (aafex). *Journal of the Air & Waste Management Association*, 62:420–430, 2012. 10.1080/10473289.2012.655884.

[37] D. P. Raymer. *Aircraft Design: A Conceptual Approach*. AIAA EDUCATION SERIES, 6^{th} edition, 1989.

[38] C. Pornet. *Conceptual design methods for sizing and performance of hybrid-electric transport aircraft*. PhD thesis, Technische Universität München, 2018.

[39] Corke. *Design of Aircraft*. Prentice Hall, 6^{th} edition, 2003.

[40] J. D. Mattingly, W. H. Heiser, , and D. T. Pratt. *Aircraft Engine Design*. AIAA EDUCATION SERIES, 2^{nd} edition, 2002.

[41] Boeing next-generation 737 (accessed: 16.12.2021). URL `https://www.boeing.com/commercial/737ng/`.

[42] Boeing 737-800 (accessed: 07.03.2021). URL `https://news.delta.com/boeing-737-800-0`.

[43] J. Cox, J. Fenouil, J. Henn, R. Hofmeister, M. Caporellie, A. S. Justin Camm, and R. Mohan. Environautics en-1. Technical report, Virginia Polytechnic Institute and State University, 2010.

[44] Detailed technical data (accessed: 27.01.2021), . URL http://www.b737.org.uk/techspecsdetailed.htm.

[45] Boeing 737–800 flight notes (accessed: 01.03.2021), . URL http://krepelka.com/fsweb/learningcenter/aircraft/flightnotesboeing737-800.htm.

[46] *737 Airplane Characteristics for Airport Planning*. Boeing Commercial Airplanes, OCTOBER 2005.

[47] E. Tulapurkara. Airplane design (aerodynamic). *Dept. of Aerospace Engg., Indian Institute of Technology, Madras*.

[48] C.-S. Lin, N. V. Dresar, and M. Hasan. A pressure control analysis of cryogenic storage systems. Technical report, Nasa, 1991.

[49] D. Verstraete, P. Hendrick, P. Pilidis, and K. Ramsden. Hydrogen fuel tanks for subsonic transport aircraft. *International Journal of Hydrogen Energy*, 35(20):11085–11098, 2010. doi: 10.1016/j.ijhydene.2010.06.060. Hyceltec 2009 Conference.

[50] D. E. Daney. Turbulent natural convection oe liquid deuterium, hydrogen, and nitrogen within enclosed vessels. *Lawrence Livermore Laboratory University of California*, 1975.

[51] F. Incropera, D. de Witt, T. Bergman, and A. Lavine. *Fundamentals of Heat and Mass Transfer*. John Wiley & Sons, 6^{th} edition, 2006.

[52] N. van Zon. Analysis of the technical feasibility of sustainable liquid hydrogen powered commercial aircraft in 2040. Technical report.

[53] A. D. Reiman. Amc's hydrogen future: Sustainable air mobility, 2009.

[54] D. Verstraete. Long range transport aircraft using hydrogen fuel. *International Journal of Hydrogen Energy*, 38(34):14824–14831, 2013. doi: 10.1016/j.ijhydene.2013.09.021.

[55] J. Markish. Valuation techniques for commercial aircraft program design. Master's thesis, Massachusetts Institute of Technology, 2002.

[56] Environmental management — life cycle assessment — principles and framework. Technical report, British Standard, 2006.

[57] Iso 14040:2006 (accessed: 08.12.2021). URL https://www.iso.org/standard/37456.html.

[58] A. Verma and A. Kumar. Life cycle evaluation of hydrogen and other potential fuels for aircrafts. *Applied Energy*, 147:556—568, 2015. 10.1016/j.apenergy.2015.03.09.

[59] Y. Bicer and I. Dincer. Life cycle assessment of hydrogen production from underground coal gasification. *International Journal of Hydrogen Energy*, 42:10722–10738, 2017. 10.1016/j.ijhydene.2016.12.119.

[60] V. authors and P. Sustainability. *SimaPro database manual - Methods library*. SimaPro, June 2020.

[61] E. Cetinkaya, I. Dincer, and G. Naterer. Life cycle assessment of various hydrogen production methods. *International Journal of Hydrogen Energy*, 37:2071–2080, 2012. doi:10.1016/j.ijhydene.2011.10.064.

[62] S. S. Kumar and V. Himabindu. Hydrogen production by pem water electrolysis – a review. *Materials Science for Energy Technologies*, 2:442–454, 2019. 10.1016/j.mset.2019.03.002.

[63] V. Fthenakis. *Practical Handbook of Photovoltaics: Fundamentals and Applications*. Elsevier, 1^{th} edition, 2003.

[64] Hydrogen pathways - updated cost, well-to-wheels energy use, and emissions for the current technology status of 10 hydrogen production, delivery, and distribution scenarios. Technical report, National Renewable Energy Laboratory, 2013.

[65] F. Calise, M. D. D'Accadia, M. Santarelli, A. Lanzini, and D. Ferrero. *Solar Hydrogen Production Processes, Systems and Technologies*. Elsevier, 1^{th} edition, 2019.

[66] Current status of hydrogen liquefaction costs. Technical report, United States Department of Energy, 2019.

[67] Jet fuel price monitor (accessed: 03.12.2021). URL `https://www.iata.org/en/publications/economics/fuel-monitor/`.

[68] Path to hydrogen competitiveness - a cost perspective. Technical report, Hydrogen Council, 2020.

[69] Easa - carbon offsetting and reduction scheme for international aviation (corsia) (accessed: 29.01.2022). URL `https://www.easa.europa.eu/eaer/topics/market-based-measures/corsia`.